PAINLESS

Energy-autonomous portable access points for infrastructure-less networks

Grant agreement no. 812991
H2020-MSCA-ITN-2018

ITN - Innovative Training Network

D3.5– Energy Harvesting techniques and network level optimisation: phase 1

WP 3 – Research Programme

Due date of deliverable:	Month 22	
Actual submission date:	30/07/2020	
Start date of project:	01/10/2018	Duration: 48 months
Lead beneficiary for this deliverable:	UCY	
Last editor:	Andreas Nicolaides	
Contributors:	Yuan Guo, Andreas Nicolaides, Muhammad Haroon Tariq, Abdelhamed Mohamed, Ioannis Krikidis	

Dissemination Level		
PU	Public	✓
PP	Restricted to other programme participants (including the Commission Services)	
RE	Restricted to a group specified by the consortium (including the Commission Services)	
CO	Confidential, only for members of the consortium (including the Commission Services)	

History table

Version	Date	Released by	Comments
V1	02.07.2020	Yuan Guo, Andreas Nicolaides, Muhammad Haroon Tariq, Abdelhamed Mohamed	Initial version
V2	12.07.2020	Christodoulos Skouroumounis	Review
V3	20.07.2020	Ioannis Krikidis	Review
V4	28.07.2020	Marco Di Renzo	Review

Table of contents

Keyword list

Energy harvesting, optimisation, 5G, intelligent reflecting surface, antenna design, network-level analysis, relaying technique

Definitions and acronyms

Acronyms	Definitions
PAINLESS	Energy-autonomous portable access points for infrastructure-less networks
ITN	Innovative Training Network
EH	energy harvesting
WPT	wireless power transfer
RF	radio-frequency
WIPT	wireless information and power transfer
WPCN	wireless powered communication network
RFID	radio-frequency identification
DL	downlink
UL	uplink
BS	base station
IoT	Internet-of-Things
M2M	machine-to-machine
WPBC	wireless powered backscatter communication
SWIPT	simultaneous wireless and information transfer
TS	time-switching
PS	power-splitting
ID	information decoding
RIS	reconfigurable intelligent surface
mmWave	millimetre wave
MISO	multiple-input single-output
PAA	parasitic antenna array

UAV	unmanned aerial vehicle
IRS	intelligent reflecting surface
UE	user equipment
LOS	line-of-sight
NLOS	non-line-of-sight
B5G	beyond 5G
DF	decode-and-forward
SNR	signal-to-noise ratio
AWGN	additive white Gaussian noise
MC	Markov chain
CSI	channel state information
MIMO	multiple-input multiple-output
AP	access point
SDR	semidefinite relaxation
SINR	signal-to-interference-plus-noise ratio
EHR	energy harvesting receiver
IDR	information decoding receiver
QoS	quality of service
CLT	central limit theorem
SAMP	single active/multiple parasitic
MAMP	multi-active/multi-passive
TbPS	threshold-based Pair Switching
HPPP	homogeneous Poisson Point Process

1. Introduction

This first (of two) phase of energy harvesting (EH) techniques and network level optimisation report is developed as part of the energy-autonomous portable access points for infrastructure-less networks (PAINLESS) project, which has received funding from the European Union, within the H2020 Marie Skłodowska-Curie Innovative Training Networks (ITNs) framework, under the 812991 Grant Agreement.

According to the objectives of Deliverable 3.5 in Work Package 3 (WP3), this report focuses on the EH techniques used in modern communication systems. The optimisation and efficient design of such techniques is investigated in this project in order to provide a reliable framework for the implementation of future self-powered networks with minimal dependence on the fixed infrastructure and by using some of the proposed 5G-enabling technologies. Therefore, for the purpose of advertising the latest breakthroughs of PAINLESS project with public, this report presents the latest research findings about radiated EH techniques that were derived in the first months of this project.

Over the past decades, wireless networks have experienced an unprecedented growth in the number of communication devices, accommodating a vastly diverse range of services and applications, such as battery-operated networks. However, battery-powered wireless devices often have energy constraints which are negatively affecting the overall performance of the network, while the replacement of the batteries can be costly, inconvenient or even impossible. As an emerging research topic, EH enables the efficient use of the available resources, and provides a new way of designing and modelling novel network architecture and protocols, aiming to prolong the lifetime of wireless communication systems. Several studies have considered conventional natural energy resources, such as solar and wind, for powering the devices [1], [2], having as main drawback the intermittent and unpredictable nature of such energy sources. On the other hand, wireless power transfer (WPT) via radio-frequency (RF) signals has been identified as a feasible solution to facilitate efficient and sustainable communication networks, as the nodes of a wireless network can harvest energy in a stable and controllable manner [3]-[5]. It is therefore one of the primary objectives of the PAINLESS project to establish a training and research platform to pioneer green, energy-autonomous portable network nodes which are self-subsistent and limitlessly-scalable, and WPT will play a pivoted role in their implementation.

However, current wireless networks have been designed for communication purposes only. Since radio waves carry both energy and information simultaneously, a unified design that integrates wireless information and power transfer (WIPT) as a single strategy is regarded as a promising approach for the development of self-sustained wireless networks [6]. It is expected that this strategy will motivate researchers to investigate technologies that go beyond conventional communication-centric wireless networks and it will enable trillions of low-power devices to be connected and powered anywhere and anytime.

WIPT can be categorized into three main technologies as follows:

- *Wireless Powered Communication Networks (WPCNs):* In such networks, all wireless powered devices are initially harvesting RF energy during the downlink (DL) period, either from a dedicated power base station (BS) or from ambient RF signals. Their harvested energy is then used in the uplink (UL) period for transferring data to their intended information receivers. WPCNs can be used in several wireless applications, such as for low-power devices in wireless sensor networks, p (IoT) and machine-to-machine (M2M) communication setups, where the manual replacement or recharging of batteries can be costly and cumbersome.
- *Wireless Powered Backscatter Communication (WPBC):* In WPBC, the energy signal is transmitted in the DL phase and the information signal is transmitted in the UL phase. In this case, backscatter modulation at a tag is used to reflect and modulate the incoming RF signal for communication with a reader. In contrast to the WPCN, the WPBC systems are simpler since the tags do not require an oscillator to generate an RF signal of their own. WPBC is typically used in radio-frequency identification (RFID) systems with passive tags.

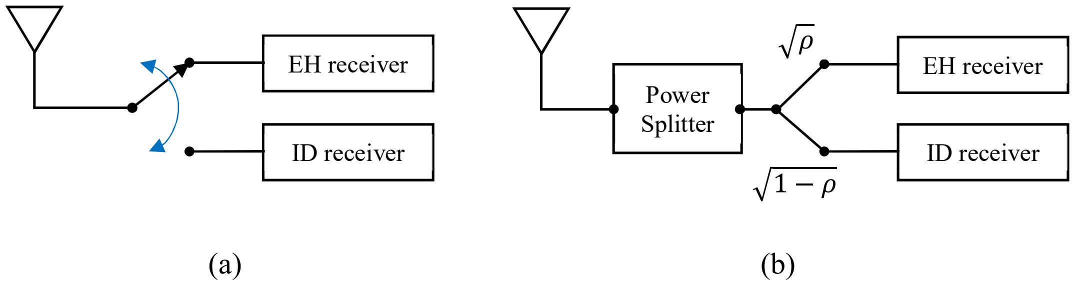

Fig. 1.1: Two receiver architectures of WIPT: (a) TS receiver (b) PS receiver.

- *Simultaneous Wireless Information and Power Transfer (SWIPT):* The concept of SWIPT, refers to the systems that use the same RF signal to provide information and energy delivery service simultaneously over a wireless DL channel. The energy and information receivers can be co-located under a single device, which is activated by harvesting energy and receiving data concurrently, or separated into two different devices, where one device is used for EH and the latter receives the information. The concept of SWIPT is a beneficial approach in cases of low-power devices which do not have access to a fixed power supply and therefore need an alternative solution for receiving both information and energy for their operation.

In practice, however, information decoding (ID) and EH cannot be performed on the same received signal. As a result, various architectures for the integrated information and energy receivers have been proposed in order to enable SWIPT or WPCN [3], [6]. The main idea behind such architectures is to separate the received signal into two distinct parts, i.e. information and energy part, either in power, time or space domain. The two most commonly adopted architectures are described below:

- *Time-switching (TS) receiver:* In this architecture, the transmission block is divided into two orthogonal timeslots, one for transferring energy and the other for conveying information. The receiver switches its operation periodically between the co-located EH and ID circuits, according to a scheduling algorithm which is synchronized with the transmitter. Despite the accurate synchronization required by such architecture, the main advantage offered by a TS-based receiver is the simple hardware implementation of the transceiver.

- *Power-splitting (PS) receiver:* In such architecture, each PS-based receiver is equipped with a power splitter which divides the received signal into two streams of different power levels, i.e. one stream with PS ratio $0 \leq \rho \leq 1$ is used for EH and the other stream, with the remaining PS ratio $1 - \rho$, is used for ID. In general, the hardware implementation of a PS receiver is a complex procedure, compared to the TS receiver. However, unlike the TS architecture, PS receivers enable the possibility of SWIPT, as the received signal can be used for EH and ID concurrently.

Despite the benefits and numerous applications introduced by WIPT technology, the concept of WIPT imposed several challenges, such as the low energy conversion efficiency, the severe path loss during WPT and the need of optimizing receiver structures in order to find the balance between EH and ID [2], [6]. It is expected that the existing network protocols and resource allocation algorithms will not be able to meet these new challenges. Aiming to address these challenges, PAINLESS researchers are currently conducting numerous new research studies, investigating the co-design of WIPT architecture with 5G-enabling techniques. More specifically, for the reduction of path loss and the enhancement of the performance both in terms of EH and ID the use of multiple relays, which are able to cooperate with each other, is considered as a low-cost and easily scalable solution. The optimization of the SWIPT technology with the aid of reconfigurable intelligent surfaces (RISs) is also taken into consideration. The appropriate design of their elements can reconfigure the propagation environment in order to improve the quality of the received signal and increase the harvested energy at the destination. Furthermore, wireless EH in millimetre wave (mmWave) cellular networks is investigated, as it seems an attractive approach which could potentially power a massive number of low-power wireless devices. Finally, the efficient design of parasitic antenna arrays (PAAs) is studied, since they can reduce the energy consumption and hardware complexity of RF circuits, and therefore enhance the energy efficiency WPT.

Throughout this report, the concept of SWIPT technology is mainly considered since is advocated as the most promising solution in implementing WPT in future communication systems. More specifically, Section 3 introduces a cooperative protocol over a multi-hop network, where the WPT is used for powering up the relaying nodes. The concept of SWIPT in the context of a RIS-based multiuser downlink multiple-input single-output (MISO) system is studied in Section 4. Moreover, in Section 5 we investigate the performance of a PAA in a rectenna for the WIPT architecture. In Section 6, we propose a novel antenna switching technique in the context of SWIPT-enabled mmWave cellular networks, and the achieved performance is investigated from a macroscopic point-of-view. For the investigation of these scenarios and the derivation of the corresponding results, a wide range of mathematical and engineering tools is used including communication theory, information theory, circuit theory, RF design, signal processing, etc. Finally, future directions regarding each one of these system scenarios are also mentioned at the end of this report.

2. System Description

PAINLESS project aims to define and demonstrate green, energy-neutral, and infrastructure-less operation for the mid- and long-term future generations of wireless networks. The main objective of this project is the design of a wireless network which can be sustained and self-organized through unreliable / intermittent / unavailable power grid provision. Moreover, the scientific breakthrough of PAINLESS lies in the paradigm shift from current dynamic wireless signal / interference management based on static power supply, to dynamic and scenario-dependent joint wireless signal / interference-and-power management. We aim to move from power grid solutions for current communication technologies to the inclusion of diverse and green power sources, such as solar, wind, electromagnetic and radio waves, etc. As illustrated in Fig. 2.1, emerging applications and devices that demand access to the network, such as terrestrial mobile terminals and unmanned aerial vehicles (UAVs), are envisioned to harvest energy from solar power or RF-signals, which could be used for signal processing and hence prolong the battery life

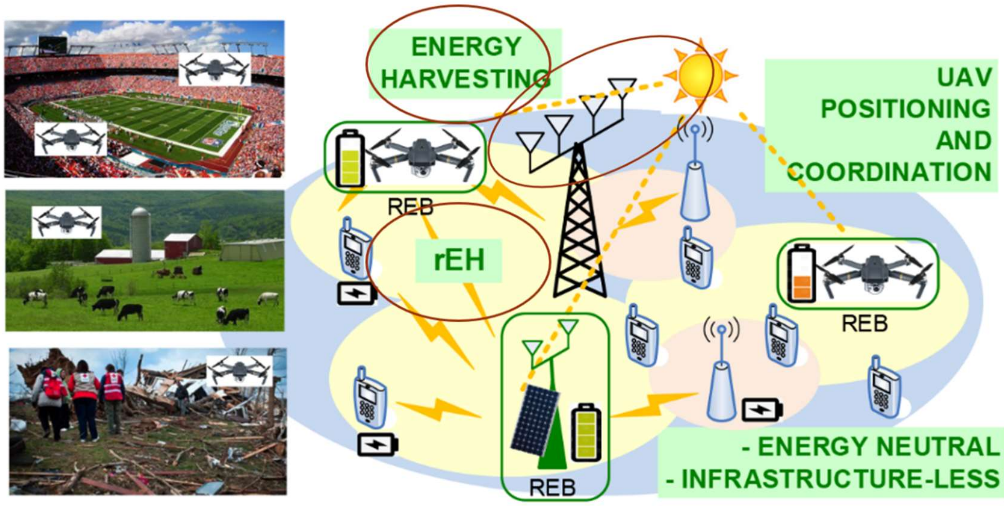

Fig. 2.1: A high-level diagram of the PAINLESS system model

time of such devices with energy constraints. To set up a power-autonomous and reconfigurable network, state-of-art techniques should be used to measure and quantify the performance of such new developed renewable energy networks. Moreover, in order to analyse the network behaviour and performance, we use stochastic geometry theory, which is a set of powerful mathematical tools enabling the statistical description of the considered deployment, from a macroscopic point-of-view.

2.1 Target Scenario

In the first phase, we consider a simple system model as shown in Fig. 2.2. The proposed system contains different network components, such as large antenna-arrays, UAVs, and intelligent reflecting surfaces (IRSs), to realize a prototype of future networks. Such emerging services are crucial for future networks in disastrous situations and scenarios where line-of-sight (LOS) communication is not feasible. The proposed study focuses on the analysis of the considered components in different scenarios. First milestone is the design of a wideband antenna array and investigate different antenna configurations in order to optimize the system performance with respect to the parameters of target scenarios. In addition, by exploiting the existence of randomly located UAVs that act as relay

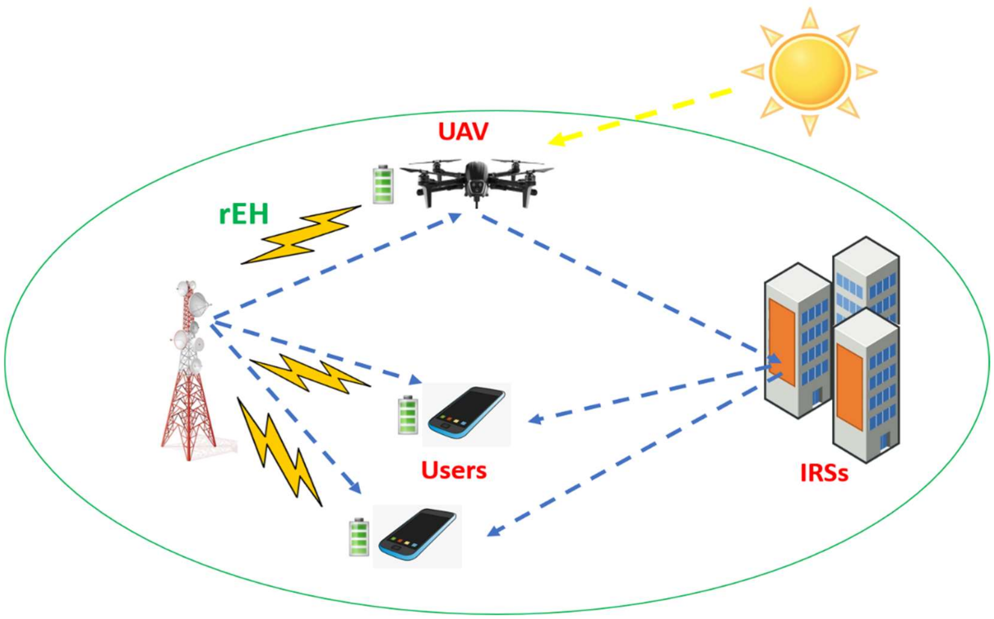

Fig. 2.2: Target WIPT scenario.

nodes, the performance of the considered system can be enhanced. Moreover, we consider the scenario where a number of IRSs are mounted on building facades, aiming to boost the quality of the link between the BS and the user equipment (UE), as well as focusing the RF signals incident upon its surface to increase the amount of harvested power. Finally, by leveraging tools from stochastic geometry, both the overall area spectral and energy efficiency are evaluated under some constraints on the harvested and consumed power. In that case, the problem formulation and solutions for communications will be analysed using UAVs as relay between the UE and multiple IRSs as an energy efficient reflector for Ground-to-Air communication.

3. WPT in cooperative multi-hop relaying networks

Although the initial deployment of 5G networks has commenced and the academia and industry partners have already made some first steps towards the beyond 5G (B5G)/6G-era, the need for denser communication networks that provide high data rates still remains. This demand is even more critical in B5G/6G networks that need to provide ultrareliable low-latency communications for massive connectivity networks in various environments. Cooperative networks with multiple relays that can assist the transmission of information from a source to a destination is a promising technology that can address the above-mentioned demand [7]. In addition to this, cooperative relay communication is a low-cost solution with high flexibility, which can help the connection of trillions of devices with enhanced reliability and low energy consumption.

However, in relaying networks each node depends on its own resources for the processing and transmission of the signals. Limitations in power can lead to non-satisfactory performance, especially if the deployment is based on poor power grid infrastructure. In the light of the above considerations, EH has gained significant research interest in recent years, as an emerging solution for prolonging the lifetime of the energy-constrained wireless devices [8]. Compared to other external natural energy sources, such as wind or solar energy, RF signals provide a more stable source for remotely powering the relaying nodes of a network, known as WPT [9]. Its application to cooperative networks is of particular importance, as it could lead to the implementation of networks which can operate in remote areas or for emergency situations detached from the power grid.

Numerous studies have investigated the performance of cooperative networks with multiple relays over a single transmission path (multi-hop relaying) [10], [11]. Another relaying technique that has received a lot of attention by the researchers is cooperative diversity, as it enables broadcast transmission and spatial diversity of the participating nodes. A cooperation scenario for multi-hop networks was introduced in [12], where the authors suggested that the spatial diversity gain could be achieved by combining at each node the signals that have been concurrently sent by all the preceding terminals along a single transmission path. However, full cooperation of the nodes in such networks exhibits a number of practical difficulties in its implementation. To overcome these issues, the authors in [13] proposed the myopic coding strategy as an information theory concept. In this strategy, each node of the network cooperates with a limited number of subsequent neighbouring nodes. They showed that the achievable rate increases considerably, while the complexity of its implementation remains low.

On the other hand, the concept of WPT in multi-hop relaying networks was not addressed until recently and therefore, there have been very few works in this topic. In [14], a multi-hop decode-and-forward (DF) system is investigated, where a source sends data to a destination with the aid of multi-hop relays under the use of the SWIPT technique. Moreover, [15] studies a nonlinear programming model to optimize multi-hop information transmission and energy transfer in a TDMA-based wireless sensor network. However, there is plenty of innovative ideas that could be investigated in this area and a plethora of new results that can be derived.

3.1 Problem formulation

For the PAINLESS project, we propose a cooperative protocol over a multi-hop network with N relays, where each relay has a buffer of finite size. The main contribution of this work is the investigation of a theoretical framework to analyse such cooperative networks in terms of outage probability and diversity gain. The protocol is based on the k-hop myopic DF coding strategy [13], where k represents the maximum number of nodes that a transmitter can forward data concurrently. The received signals of each relay are stored in a buffer b_i of finite size $L_i = \min(k, N - i + 1)$ which is used as a one-dimensional array with indexed elements, where the element $b_i[w], 1 \leq w \leq L_i$, refers to the w-th most recently received signal. We assume that a signal at the receiver is successfully decoded if the instantaneous signal-to-noise ratio (SNR) is not below a predefined threshold γ, otherwise an outage occurs. For this, a one-dimensional array β_i is introduced that indicates which of the received signals stored in the buffer b_i were successfully decoded. Therefore, the transmission of the decoded signals to the appropriate nodes is adapted according to the status of the arrays β_i.

Each relay is activated by harvesting energy from a BS Ψ, which is used as a power beacon, and uses its harvested energy for forwarding its decoded signals, as it is shown in

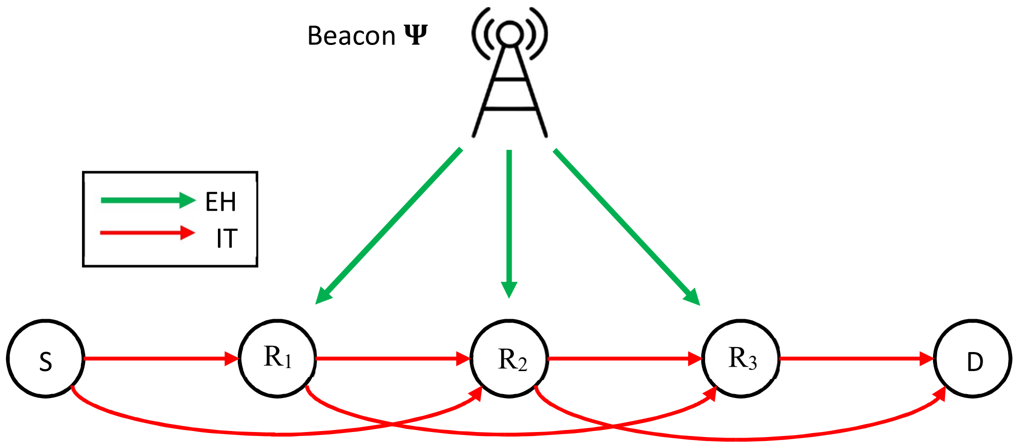

Fig. 3.1: Topology for 2-hop myopic DF strategy in a wireless network with three relays.

Fig. 3.1. For this, the TS technique is used [6], where for each time-slot the relays dedicate a portion of that time for EH and the rest of the time-slot for transferring the decoded signals. A relay can forward data only if its harvested energy is at least equal to a predefined threshold, otherwise it remains idle and stores the harvested energy for the next time-slot. Finally, for the analysis we consider independent and identically distributed (i.i.d.) channel links that experience propagation path loss and fading modelled as frequency-flat Rayleigh block fading.

The first phase of this work is focused on the information transfer part, so for the rest of this section we assume that the relays are always active and transmit data with the same transmit power P (dB). Therefore, the instantaneous SNR at a receiver j during one time-slot, assuming that the transmission at every link is coherent, is given by

$$SNR_j = \frac{1}{\sigma^2}\left(\sum_{i=0}^{N} \mathbb{1}_{i,j}\left|h_{i,j}\right|\sqrt{d_{i,j}^{-\eta} a_{i,j} P}\right)^2,$$

where σ^2 is the variance of the additive white Gaussian noise (AWGN) at the receiver, $\left|h_{i,j}\right|$ is a random variable that follows a Rayleigh distribution with unit scale parameter, $d_{i,j}$ is the distance between the nodes i and j, η denotes the path loss exponent, $a_{i,j}$ is the power splitting parameter and $\mathbb{1}_{i,j}$ equals to one if node i transmits a signal to node j at the current time-slot, otherwise it is equal to zero.

For the analysis of this system we investigate a theoretical framework that models the evolution of the relays' buffers as a Markov chain (MC). For this, we construct the state transition matrix $\boldsymbol{A}$ and derive the stationary distribution $\boldsymbol{\pi}$ of the MC, which will be used for the computation of the system's outage probability. A state of the MC is formed by the concatenation of all the arrays β_i. Thus, each state is a vector of finite size $\sum_{i=1}^{N} L_i = (2N - k + 1)\frac{k}{2}$, that represents which elements in each buffer have decoded signals. With a slight abuse of notation, we let

$$s_m \triangleq (\beta_{1,m}\ \beta_{2,m}\ \cdots\ \beta_{N,m}),$$

denote the m-th state of the MC, $1 \leq m \leq M$, where M is the number of the states. The entries of the state transition matrix are then given by

$$p_{r,q} = \begin{cases} \prod_{j=1}^{N} \left[\beta_{j,r}[1]\left(1 - P_o(T_{j,q})\right) + (1 - \beta_{j,r}[1]) P_o(T_{j,q})\right], if\ s_q \to s_r\ exists; \\ 0, otherwise, \end{cases}$$

where $P_o(\cdot)$ is the probability of having an outage event, and $T_{j,q}$ is the set of nodes that transmit a signal to the relay j, given that s_q was the previous state. The probability of having an outage event at the j-th node, using the Gil-Pelaez inversion theorem [16], is

$$P_o(T_{j,q}) = \frac{1}{2} - \frac{1}{\pi}\int_0^{\infty} \frac{1}{t} \Im\left[\exp\left(-it\sqrt{\frac{\gamma\sigma^2}{P}}\right) \prod_{i=\max(0,j-k)}^{j-1} \left(\varphi_{i,j}(t)\right)^{\beta_{i,q}[j-i]}\right] dt,$$

where $\Im(x)$ returns the imaginary part of x, i denotes the imaginary unit and $\varphi_{i,j}(t)$ is the characteristic function of $|h_{i,j}|$ and is equal to

$$\varphi_{i,j}(t) = 1 + 2it\sqrt{\frac{\pi a_{i,j}}{2d_{i,j}^{\eta}}} \exp\left(-\frac{a_{i,j}t^2}{2d_{i,j}^{\eta}}\right)\left[1 - Q\left(it\sqrt{\frac{a_{i,j}}{d_{i,j}^{\eta}}}\right)\right].$$

The outage probability of the system $P_{out}(\gamma)$ can be calculated by using the steady state of the MC along with the probability of an outage event at the destination. Thus, $P_{out}(\gamma)$ can be expressed as

$$P_{out}(\gamma) = \min_{\{a_{ij}\}} \sum_{m=1}^{M} \pi_m P_o(T_{N+1,m}).$$

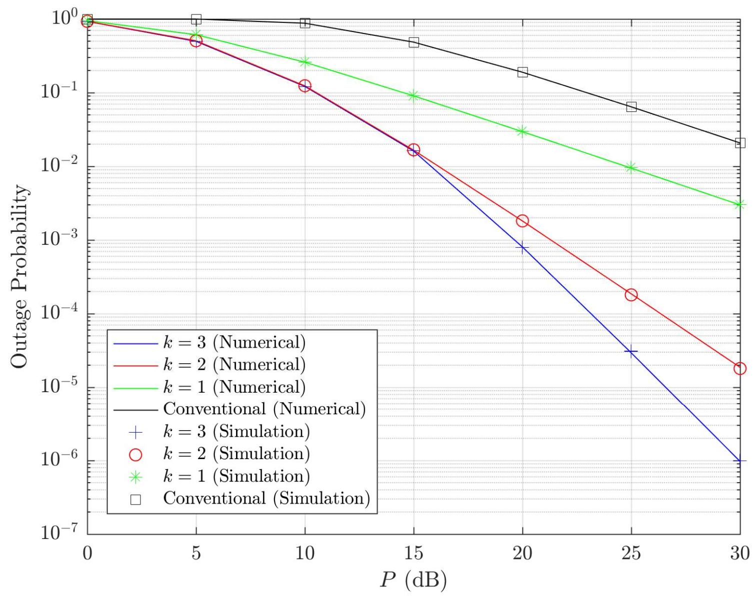

(a)

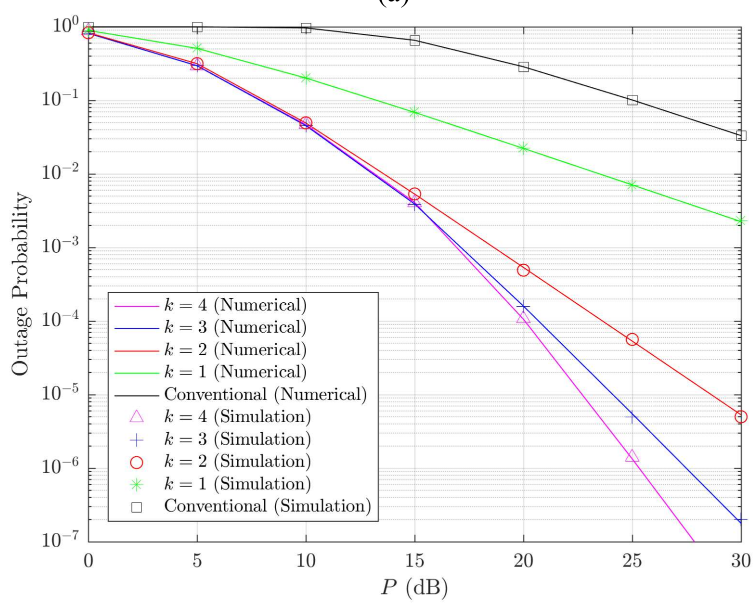

(b)

Fig. 3.2: Outage probability versus P for a network topology with (a)$N = 2$ and (b)$N = 3$ relays, $k = 1, \dots, N + 1$ and $\gamma = 0$ dB.

3.2 Numerical results

Fig. 3.2 illustrates the system's outage probability against the transmit power P for all possible scenarios in a network setting with (a)$N = 2$ and (b)$N = 3$ relays. Our results are numerically optimized with respect to the power splitting parameters a_{ij}. We observe that our proposed protocol outperforms the conventional multi-hop model, where each node sends a signal only to its subsequent node through orthogonal channels. Furthermore, the figure shows that an increase in the number of hops results in an improvement of the outage probability performance, with the cases of $k = 1$ and $k = 2$ revealing the most significant difference. In addition, it can be seen that as the number of hops increases the diversity gain is also improved, which complies with our analysis indicating a diversity order equal to k. Finally, we can see that the theoretical values perfectly match to the simulation results and this observation validates the accuracy of our analysis.

4. Optimisation in RIS-Aided SWIPT

The primary purpose of the WIPT is to exploit the radio wave signals which carry information and energy to make the best use of the spectrum and radiation as well as the current infrastructure of the wireless communication system. Energizing electronic devices through radio wave EH has two major classes based on the transmission distance, which are Near-field and Far-field. There are now many commercial products that exploit the Near-field inductive technology for powering devices wirelessly, but it is limited for a small range. Transferring energy for a long distance is referred to as Far-field. Due to the advancements of circuit design and the low-power requirement of modern devices as well as the massive increase of IoT devices, WPT has been raised as a promising paradigm for feeding such devices with the required energy. WIPT has many potentials and new opportunities such as no wires, batteries, reliability, on-demand and mobility, but also it brings new challenges and related problems to be solved, like efficiency, coverage, mobility support, health and safety issues [6].

SWIPT has emerged as a promising solution for providing the required energy of low-power hungry future IoT networks, which would have a significant impact on enhancing energy efficiency. However, deploying more BSs with multi-array antennas as well as its

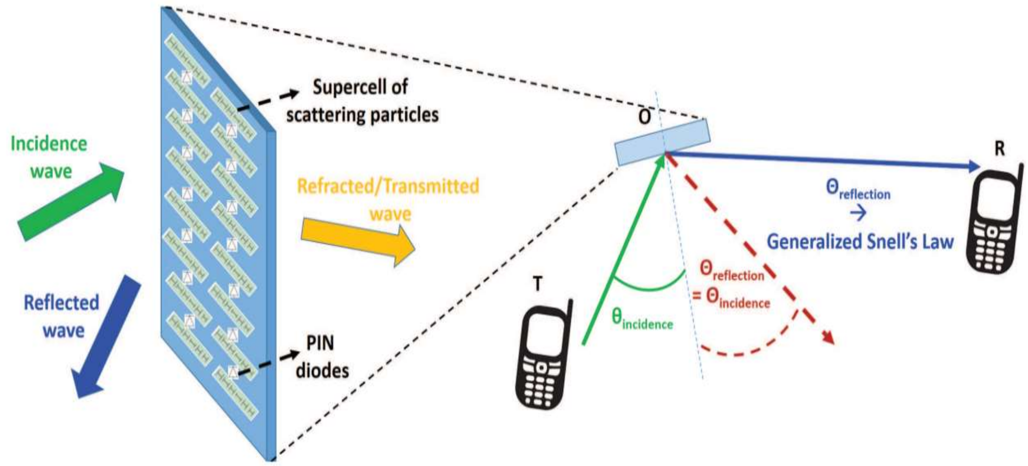

Fig. 4.1: The working principle of RIS.

energy-hungry RF chains will increase the total cost of installation and maintenance processes as well as the energy bill due to the power consumed by RF chains. RISs [17], [18], have been emerged a new cost-effective, and spectrum-energy high data rates techniques for the next generation of wireless communication systems. The idea behind RIS and its capability of reconfiguring the propagation environment (wireless channel) rely on the physical properties of its Meta-Materials building blocks. A large number of these building blocks often referred to as unit-cells or meta-atoms, are assembled into a planner surface. Fig 4.1 shows the working principals of RIS, where the incident electromagnetic signals can be reflected, refracted, or absorbed based on the available channel state information (CSI) and the targeted application. Each reflecting element is designed and controlled in such a way to have the capability of reconstructing the characteristic of the electromagnetic waves impinging upon its surfaces such as amplitude, phase, and polarization. Thereby, it yields a punch of constructive signals at the intended receiver or destructive signals at the unintended receiver. To enhance the communication link quality such as the quality of the received signal and the amount of harvested energy, the RIS should be programmed based on the available CSI at the BS to allow the signals to be constructively added at the desired receiver. On the other hand, the destructive manner is applied to create a free-interference zone and security reasons at unintended receivers.

RIS is considered as an array of passive antenna elements with a lightweight, which enables it to be easily deployed on the building facades and walls with negligible power consumption compared to enormous energy required for the RF chains of Massive multiple-input-multiple-output (MIMO) antennas arrays.

There have been various approaches to exploiting the full potential benefits of RIS. Through jointly optimizing the transmit beamforming at Access Point (AP) and the phase shift-vector (Passive beamforming) at RIS under various wireless communication scenarios seeking for the enhancement of the transmission link quality to produce an energy-spectrum efficient communication system. In [19], the problem of maximizing the received energy at UE was studied, where the authors proposed a semidefinite relaxation (SDR) method to find a suboptimal solution to reflection coefficient at RIS and transmit beamforming at AP. In [20], the fixed point iteration method was proposed to reduce the SDR method complexity. The Weighted Sum Rate maximization was studied in [21] under perfect CSI, and the authors extended their method to cover the case when the perfect CSI is not available. Robust beamforming design for minimizing the total transmit power of a multi-user MISO subject to imperfect CSI constraints was studied in [22]. The authors in [23], investigated the problem of maximizing the sum rate of all the multicasting group in a downlink RISs-aided system by proposing two efficient Majorization-Minimization (MM) based algorithms. In [24], the authors studied the problem of maximizing the minimum signal-to-interference-plus-noise ratio (SINR) at UEs for a RISs- assisted massive MIMO communication system. A globally optimal solution for jointly optimizing transmit precoding matrix and passive beamforming based on the Branch-and-Bound algorithm was proposed in [25].

CSI is playing a critical role in designing and programming the RIS. The authors in [26] studied channel estimation of downlink single cell of a RIS-assisted multiuser MISO

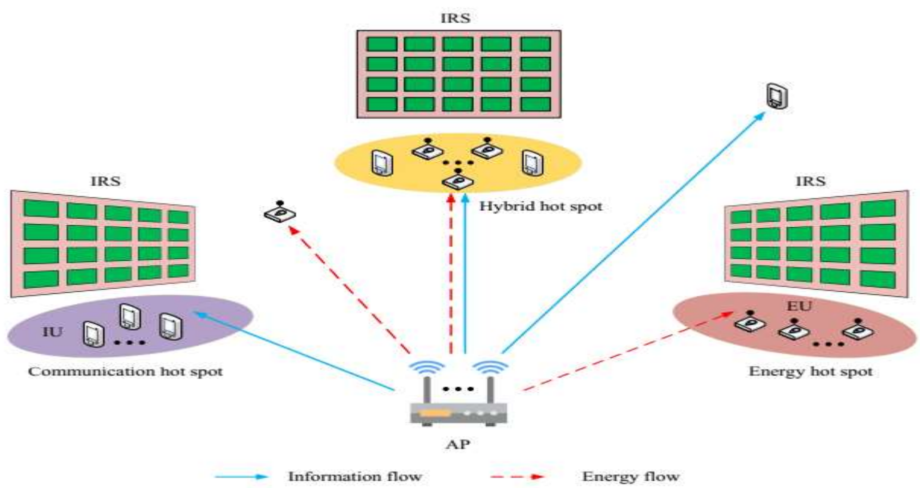

Fig. 4.2: Application of RIS for improving SWIPT system performance.

communication system. The authors adopt the PARAllel FACtor (PARAFAC) decomposition method to unfold the resulting cascaded channel. An iterative channel estimation procedure has been presented to estimate the direct channel between the BS and RIS, as well as the virtue channels between RIS and users. In [27], the authors modify the passive RIS architecture by adding only an active RF chain for baseband reception besides the comprised passive unit elements. With this novel design in hand, the RIS can now perform channel estimation on its side. Moreover, by exploiting channel sparsity of the spatial domain, an alternating optimization-based algorithm was presented to estimate the cascaded propagation channel.

Despite the achievements of employing RF signal for SWIPT, the low efficiency of far-field WPT still stands up. As the energy harvesting receivers (EHRs) require more received energy than the information decoding receivers (IDRs), invoking RIS with its capability to focus the reflected signals incident on its surface will help to create an Energy Spot Zone, which has emerged as a bright solution for alleviating energy-rate trade-off and far-field problem. Fig 4.2 shows RIS's potential application where the RIS can be mounted in a nearby position to help create an energy/information/hybrid hot spot zone aiming to improve the communication link quality.

Wu et al. [28] investigated the problem of maximizing the total received power at EHRs subject to a set of individual SINR constraints at IDRs for multi-user RIS-Aided SWIPT system. An SDR-based algorithm has been presented to obtain a sub-optimal solution of jointly optimizing transmit and reflecting beamforming vectors. Besides, it has been proved that sending a separate energy-bearing signal is not required, and the transmitted information-carrying signal is sufficient. On the other side, the authors in [29] proposed to transmit a-priori known pseudo-random sequences energy signal at multi-antenna BS. At the same time, the IDRs receivers can efficiently suppress the resultant interference. Under this assumption, the authors adopted the SDR technique for jointly optimizing both transmit beamforming and phase shift-vector at RIS. Alternately, to maximize the minimum harvested power by all EHRs under SINR constraints at IDRs and maximum transmit power budget for the Multiuser MISO SWIPT system. The numerical results showed that sending an energy signal besides utilizing RIS is crucial for multiuser SWIPT systems performance enhancement. The problem of minimizing the transmitted power at multi-antenna BS subject to Quality of Service (QoS) conditions, such as SINR at IDRs and the harvested energy constraints at EHRs, was introduced in [30]. The authors propose a penalty-based algorithm as an efficient iterative method to reduce the computational complexity of the alternating optimization technique used for many QoS constraints after applying a proper transformation of the QoS constraints. However, the extra EH constraint added to the unit modulus constraint and total transmit power budget make the optimization problem more challenging because of the non-convex EH constraints. The solution may be infeasible due to the conflicting constraints.

4.1 Problem Formulation

System model

Consider an RIS-based multiuser downlink MISO of a SWIPT system, where we have a BS equipped with M antennas to serve K_E EHRs and K_I IDRs, each equipped with a single antenna. This downlink communication is performed with the aid of a RIS that is composed of N reflecting elements. Let us assume that all channels have a quasi-static flat fading. The baseband equivalent channels from AP to the RIS, form AP to K-th IDR, from AP to l-th EHR, from the RIS to the k-th IDR, from the RIS to the l-th EHR are denoted by $D \in \mathbb{C}^{N\times M}, h_{d,k} \in \mathbb{C}^{1\times M}, g_{d,l} \in \mathbb{C}^{1\times M}, h_{r,k} \in \mathbb{C}^{1\times N}, g_{r,l} \in \mathbb{C}^{1\times N}$, respectively. Let us define the diagonal phase shift matrix at RIS as $\Theta = diag(\theta_1, \ldots, \theta_n, \ldots, \theta_N) \in \mathbb{C}^{N\times N}$, where $\theta_n = e^{j\varphi_n}$ is the phase of the n-th reflecting element of RIS. The transmitted signal at the AP can be expressed as:

$$x = \sum_{k=1}^{K} w_k s_k ,$$

where $w_k \in \mathbb{C}^{M\times 1}$ represents the transmit beamforming vector for the k-th IDR user and $s_k \sim \mathcal{CN}(0,1)$ is the transmit data symbol for the k-th IDR user, which is assumed to be independent random variable with zero mean and unit variance with $\left[s_k s_k^H\right] = 1$, $\left[s_i s_j^H\right] = 0$ for $i \neq j$. The received signal at the k-th IDR user can be denoted by

$$\begin{aligned} y_{I,k} &= h_{d,k} x + h_{r,k} \Theta D x + n_{I,k} \\ &= (h_{d,k} + h_{r,k} \Theta D) \sum_{k=1}^{K} w_k s_k + n_{I,k}, \end{aligned}$$

where $n_{I,k} \sim \mathcal{CN}(0, \sigma_I^2)$ is the $AWGN$ vector at the k-th IDR user. By the same way, the received signal at the l-th EHR user is expressed as

$$\begin{aligned} y_{E,l} &= g_{d,l} x + g_{r,l} \Theta D x + n_{E,k} \\ &= (g_{d,l} + g_{r,l} \Theta D) \sum_{k=1}^{K} w_k s_k + n_{E,k}, \end{aligned}$$

where $n_{E,l} \sim \mathcal{CN}(0, \sigma_E^2)$ is the $AWGN$ vector at the l-th EHR user. Let us define $\theta = [\theta_1, \ldots, \theta_N]$, $H_{r,k} = diag(h_{r,k}) D$, $G_{r,l} = diag(g_{r,l}) D$, then the equivalent channel spanning from the AP to the k-th IDR user can be denoted by $H_k = h_{d,k} x + h_{r,k} \Theta D$ $= h_{d,k} + \theta^H diag(h_{r,k}) D$ and the received signal by the k-th IDR user can be denoted by

$$\begin{aligned} y_{I,k} &= H_k \sum_{k=1}^{K} w_k s_k + n_{I,k} \\ &= H_k w_K s_k + \sum_{i=1, i\neq k}^{K_I} H_k w_i s_i + n_{I,k} . \end{aligned}$$

Similarly, for the l-th EHR user, let us define its equivalent channel as $G_l = g_{d,l} + \theta^H diag(g_{r,l})D$. Then, the received signal at the receiver of the l-th EHR user can be expressed as

$$y_{E,l} = G_l \sum_{k=1}^{K} w_k s_k + n_{E,l}.$$

The SINR for the k-th user can be given as

$$\gamma_{I,k} = \frac{\left|\left(h_{d,k} + \theta^H H_{r,k}\right) w_k\right|^2}{\sum_{i=1, i\neq k}^{K_I} \left|\left(h_{d,k} + \theta^H H_{r,k}\right) w_i\right|^2 + \sigma_{I,k}^2},$$

and the achievable date rate of the k-th IR can give as

$$\begin{aligned} R_k(w,\theta) &= \log(1+\gamma_k) \\ &= \log(1+\frac{w_k^H H_k^H H_k w_k}{\sum_{i=1, i\neq k}^{K_I} w_i^H H_k^H H_k w_i + \sigma_k^{\ 2}}) \\ &= \log(1+ w_k^H H_k^H H_k w_k J_k^{-1}), \end{aligned}$$

where $J_k^{-1} = \sum_{i=1, i\neq k}^{K_I} w_i^H H_k^H H_k w_i + \sigma_k^{\ 2}$ represents the value of the interference-plus-noise. On the other hand, and for simplicity, we will consider a simple linear EH model, where the harvested power by EHR is proportional to the total received power while ignoring the noise power. As a result, the total power harvested by the l-th user, denoted by Q_l, is given by

$$Q_l = \rho tr(\sum_{k=1}^{K_I} w_k^H G_l^H G_l w_k),$$

where $0 \leq \rho \leq 1$ represents the efficiency of the EH circuit for converting the RF-signal into a direct current. Then, the total energy harvested, denoted by Q, can be expressed as

$$
\begin{aligned}
Q &= \sum_{l=1}^{K_E} Q_l \\
&= tr\left(\sum_{k=1}^{K_I} w_k^H \left(\sum_{l=1}^{K_E} \rho G_l^H G_l) \right) w_k \right) \\
&= tr\left(\sum_{k=1}^{K_I} w_k^H G w_k \right),
\end{aligned}
$$

where $G = \left(\sum_{l=1}^{K_E} \rho G_l^H G_l) \right)$. We adopt the constraint of the total harvested power by all EHR to be higher than a predefined minimum power threshold denoted by $\bar{Q}$, thus,

$$
Q = tr\left(\sum_{k=1}^{K_I} w_k^H G w_k \right) \geq \bar{Q}.
$$

Problem statement

We aim to maximize the weighted sum rate (WSR) of all IR users subject to the transmit power budget, unit modulus constraint for the phase shift at RIS, and the total harvested power constraint to be higher than the threshold value. We aim to perform this task by jointly optimizing the transmit beamforming at the AP and the passive beamforming of RIS. As the RIS is a passive element, the AP is responsible for performing the calculation for optimizing the phase-shift vector; then, this control information is to be sent to the RIS controller through a dedicated wireless channel. The WSR maximization problem can be formulated as

$$
\begin{aligned}
&\max_{w,\theta} \sum_{k=1}^{K_I} \omega_k R_k(w,\theta) \\
&\text{s.t.} \ \sum_{k=1}^{K_I} \left\| w_k \right\|^2 \leq P_T, \\
&\quad tr\left(\sum_{k=1}^{K_I} w_k^H G w_k \right) \geq \bar{Q}, \\
&\quad \left| \theta_n \right| = 1, n = 1, \ldots, N,
\end{aligned}
$$

where the weight ω_k assigned to each user represents the priority for scheduling the IR users, P_T is the maximum transmitted power budget and the last constraints the Unit-Modulus constraint for each reflecting element of RIS.

Due to the non-convex nature of the objective function because of the high coupling between the optimization variables w_k and θ. Besides, the non-convex EH constraint makes the optimization problem more challenging to solve. In addition to the conflicting nature between the first and second constraints, the optimization problem may be infeasible.

4.2 Random Rotation-based Low-Complexity Schemes for IRSs

Most of the recent works, focus on optimizing the incident signal's phase shifts at the IRS and assume knowledge of the channel state information. However, this corresponds to higher complexity and power consumption but can also be impractical in some cases. In this subsection, we propose two low-complexity and energy efficient techniques for IRS-aided communications, namely, a coding-based and a selection-based scheme, both based on random phase rotations. In particular, the coding-based scheme uses time-varying random phase rotations to produce a time-varying channel. The selection-based scheme, selects and activates a partition of the IRS elements at each time slot based on the received signal power at the destination.

More specifically, we consider an IRS-aided network, where a source S achieves communications with a destination D through the employment of an IRS with M reflecting elements, as shown in Fig. 4.3. The source and destination are equipped with a single antenna and a direct link between them is not available (e.g., due to obstacles). A codeword $\boldsymbol{X} \triangleq [x_1, x_2, \cdots, x_T], x_T \in \mathbb{C}, 1 \leq t \leq T$, is transmitted by the source over T symbols time; we assume that $T < M$. All wireless links are assumed to exhibit Rayleigh fading; we define by h_i and g_i the fading coefficients from S to the i-th element and from the i-th element to D, respectively. The fading coefficients remain constant during the T transmissions but change independently every T channel uses according to a complex

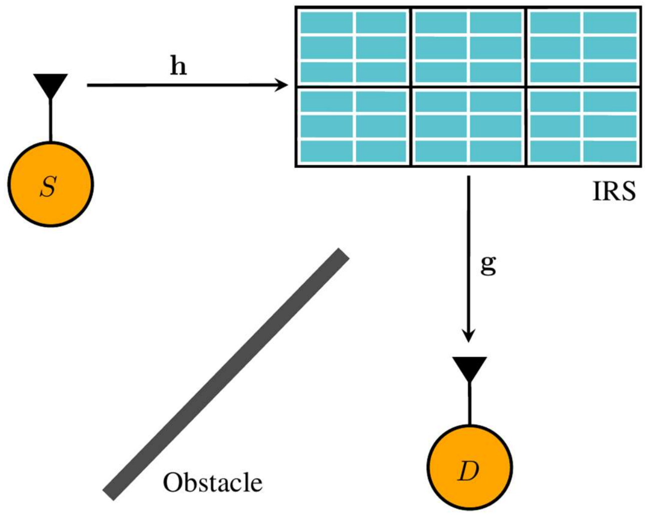

Fig. 4.3: The considered IRS-aided communication network.

Gaussian distribution with zero mean and unit variance, i.e. $h_i \sim \mathcal{CN}(0,1)$ and $g_i \sim \mathcal{CN}(0,1)$.

We assume that knowledge of any channel state information does not exist. At every time instant t, each element of the IRS, randomly rotates (shifts) the phase of the incident signal. Let

$$\boldsymbol{\Phi}_t = diag\left[\exp\left(i\varphi_{t,1}\right)\ \exp\left(i\varphi_{t,2}\right)\ \cdots\ \exp\left(i\varphi_{t,M}\right)\right],$$

be the diagonal matrix containing the independent and identically distributed phase shift variables. Due to the random rotations, the variables $\varphi_{t,i}$ are uniformly distributed in $[0,2\pi)$. Therefore, if the source transmits with a constant power P, the received signal at the destination D at the t-th channel use can be written as

$$r_t = \sqrt{P}\boldsymbol{h}^T\boldsymbol{\Phi}_t\boldsymbol{g}x_t + n_t,$$

where $\boldsymbol{h} = [h_1\ h_2\ \cdots\ h_M]^T, \boldsymbol{g} = [g_1\ g_2\ \cdots\ g_M]^T$, and $n_t \sim \mathcal{CN}(0,\sigma^2)$ is the additive white Gaussian noise with variance σ^2. Then, the instantaneous SNR at the destination D over the t-th transmission is

$$\gamma_t = \frac{P}{\sigma^2} H_t,$$

where $H_t = \left|\sum_{i=1}^{M} h_i g_i \exp(\imath \varphi_{t,i})\right|^2$, is the channel gain from the M elements of the IRS. The performance of the proposed protocols is analysed in terms of outage probability and energy efficiency. In general, the outage probability is given by

$$\Pi(\rho, T) = \mathbb{P}\left\{\frac{1}{T}\sum_{t=1}^{T} \log_2(1+\gamma_t) < \rho\right\},$$

where ρ is a non-negative pre-defined threshold, and the end-to-end energy efficiency is equal to

$$\eta = \frac{\mathbb{E}\left\{\frac{1}{T}\sum_{t=1}^{T} \log_2(1+\gamma_t)\right\}}{P_c},$$

where P_c is the system's total power consumption.

Coding-based scheme

In the coding-based scheme, the destination receives the superposition of M independent channels at each time instant t. The different phase shifts induced by the IRS elements at each time slot introduce an artificial fast fading channel, which can increase the performance, without any knowledge regarding the channel at the source, the IRS or the destination. Note that the instantaneous SNRs between different time slots are correlated. As this makes the derivation of the outage probability challenging, an approximation under the central limit theorem (CLT) is given, which is sufficient and appropriate to describe the proposed scheme's behaviour. Therefore, the outage probability of the coding-based scheme, under the CLT, is approximated by

$$\Pi_{CB}^{CLT}(\rho, T) \approx \left(\frac{\sigma^2}{MP}\right)^{T-1} \int_1^{\xi_T} \cdots \int_1^{\xi_2} \left(1 - \exp\left(-\frac{\Theta}{M}\right)\right) \prod_{t=2}^{T} \exp\left(-\frac{\sigma^2}{MP}(w_t - 1)\right) dw_2 \cdots dw_T,$$

where $\xi_i = 2^{\rho T} / \prod_{t=i+1}^{T} w_t$, $2 \leq i \leq T$, and

$$\Theta \triangleq \frac{\sigma^2}{P}\left(\frac{2^{\rho T}}{\prod_{t=2}^{T} w_t} - 1\right).$$

By using this approximated expression, it follows that the coding-based scheme achieves time diversity of order T with coding gain G_{CB} equal to

$$G_{CB} = \left(\frac{\sigma^2}{M}\right)^T (-1)^T \left(1 - 2^{\rho T} \sum_{t=0}^{T-1} \frac{(-1)^t}{t!} \log^{\mathrm{t}}(2^{\rho T})\right),$$

which follows by evaluating the $(T-1)$-fold integral and after some trivial algebraic manipulations. The expected rate achieved by the coding-based scheme is

$$R_{CB} = \frac{2}{\Gamma(M)} \int_0^\infty \left(\frac{\theta\sigma^2}{P}\right)^{\frac{M}{2}} K_M\left(2\sqrt{\frac{\theta\sigma^2}{P}}\right) d\rho,$$

where $\theta \triangleq 2^\rho - 1, K_M(\cdot)$ is the modified Bessel function of the second kind of order M and $\Gamma(\cdot)$ is the complete gamma function. Finally, the energy efficiency achieved by the coding-based scheme is

$$\eta_{CB} = \frac{R_{CB}}{P/\xi + P_S + P_D + P_{IRS}},$$

where ξ is the amplifier's efficiency, whereas P_S, P_D and P_{IRS} is the static power consumption at the source, destination and IRS, respectively. The power consumption at the IRS depends on the number of activated elements, that is, $P_{IRS} = MP_E$, where P_E is the power consumed to operate a single element.

Selection-based scheme

For the selection-based scheme, we consider $T = 1$ and assume that the IRS is partitioned into N non-overlapping sub-surfaces of m elements, where N is a divisor of M, i.e. $mN = M$. An example of the system model is illustrated in Fig. 1 with $N = 6$ and $m = 6$, where the partitions are shown by the solid lines. We assume there is knowledge of the received SNR power at the destination from each sub-surface; this can be implemented by a training period, where the received signal strength indicator (RSSI) is fed back to the IRS controller. Then, at each time slot, the IRS controller selects and activates the sub-surface which achieves the highest SNR at the destination. For this scheme, the outage probability is equal to

$$\Pi_{SB}(\rho) = \Pi(\rho, 1)^N,$$

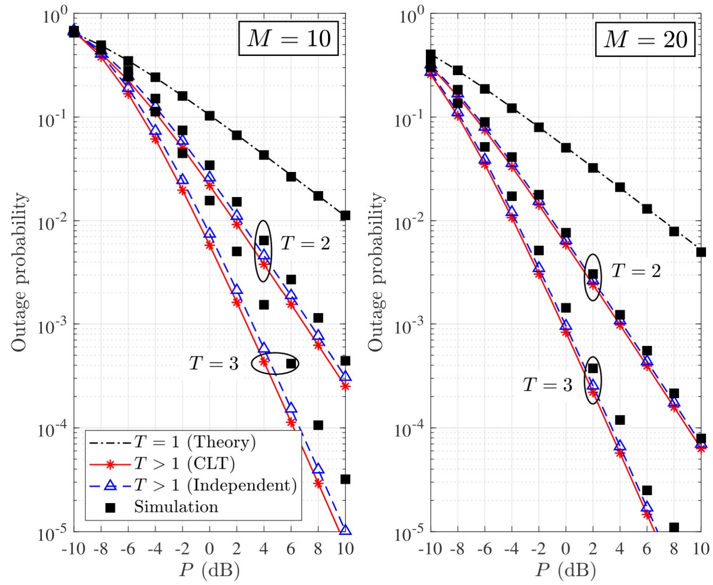

Fig. 4.4: Outage probability versus P for the coding-based scheme.

where N is the number of sub-surfaces with m elements and $\Pi(\rho, 1)$ is the outage probability of a random selection for $T = 1$ and $M = m$. Once again, by using the approximation of CLT, it can be seen that the selection-based scheme achieves full spatial diversity order with coding gain equal to

$$G_{SB} = \left(\frac{\sigma^2}{m}\right)^N (2^\rho - 1)^N.$$

The expected rate achieved by the selection-based scheme is

$$R_{SB} = N \int_0^\infty \log_2\left(1 + \frac{P}{\sigma^2} h\right) F_H(h)^{N-1} f_H(h) dh,$$

where $f_H(h) = 2h^{(M-1)/2} K_{M-1}(2\sqrt{h}) \Gamma^{-1}(M)$ and $F_H(h) = 1 - 2h^{M/2} K_M(2\sqrt{h}) \Gamma^{-1}(M)$. Therefore, the energy efficiency achieved by the selection-based scheme is

$$\eta_{SB} = \frac{R_{SB}}{P/\xi + P_S + P_D + P_{IRS}},$$

where the power consumption parameters are defined as before but with $P_{IRS} = mP_E$, since only m elements are activated at each time slot. It is clear, that $\eta_{SB} = \eta_{CB}$ when

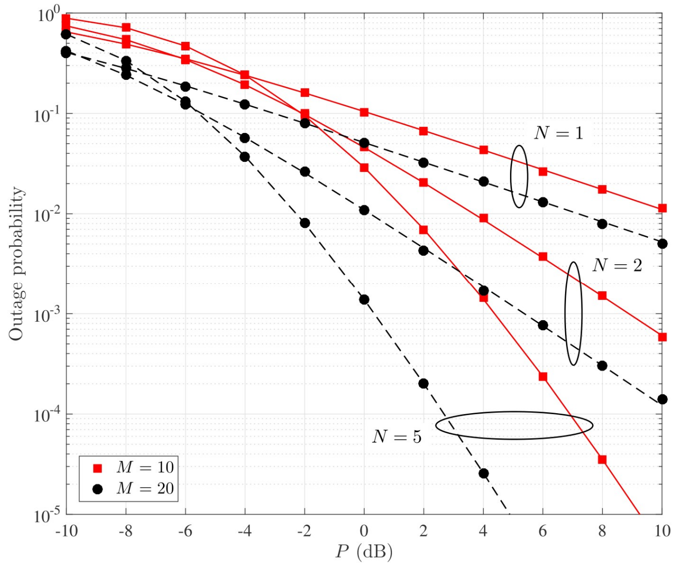

Fig. 4.5: Outage probability versus P for the selection-based scheme.

$N = T = 1$. For $N = T > 1$, the denominator of η_{SB} is always less that the one of η_{CB}, since $m < M$.

Fig. 4.4 depicts the outage probability achieved by the coding-based scheme in terms of the transmit power P, the number of channels uses T and the number of reflecting elements M. As expected, the performance is improved with an increase of M. Moreover, and most importantly, increasing the number of channels uses T provides significant gains to the outage probability. Also, we can observe that the scheme provides full diversity order T, as deduced by our analysis. Finally, the figure validates the considered assumptions and approximations of our theoretical study.

Fig. 4.5 illustrates the performance of the selection-based scheme with regards to the number of reflecting elements M and the number of sub-surfaces N. It is clear that the selection process improves the performance as N increases, especially in the high SNR regime, where the scheme achieves full spatial diversity order. Again, the theoretical and simulation results are in agreement, which validates our analysis.

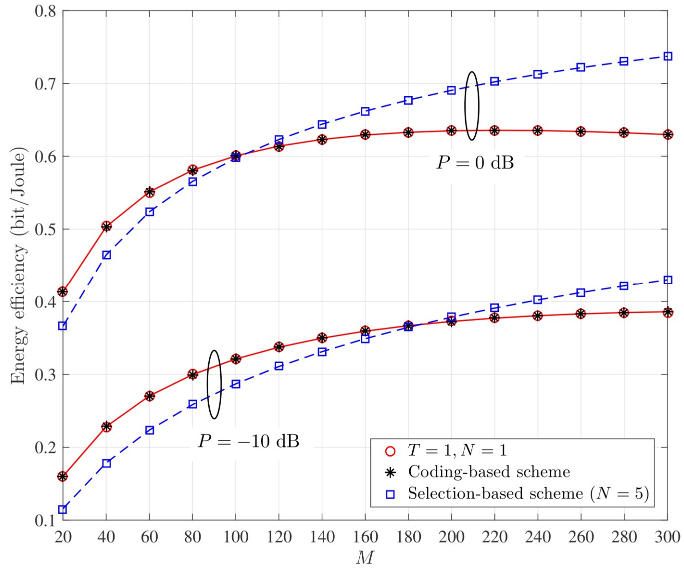

Fig. 4.6: Energy efficiency versus number of elements M.

Finally, Fig. 4.6 shows the energy efficiency of the proposed schemes for different values of M and P. The first main observation, is that the energy efficiency initially increases with M but at some point, it starts to decrease. This is expected, since more active elements implies higher rate but, at the same time, higher power consumption. Since the power consumption increases linearly, at some point, the rate-to-power-consumption ratio decreases. Secondly, the energy efficiency of the coding-based scheme is the same as with the conventional case ($T = 1$). This is because, on average, the rates of the two scenarios are equal. Finally, the selection-based protocol has a smaller energy efficiency for small values of M, compared to the other two cases. However, as M increases, the selection-based scheme becomes more energy efficient due to the fact that it activates a fraction of the available elements at the IRS; this is clearly more evident for $P = 0$ dB.

5. PAAs based on reduced energy consumption

The future demands for energy-autonomous, infrastructure-less networks have increased with the demands of high-speed data communications. This led the research community focus on an interesting topic of wireless power. The new research fascination is no wires, no contacts, no batteries, and reliable energy supply, but the challenges also emerge to provide autonomous power networks, energy limited communication devices. The research brings up new challenges and calls up the research community for integration of various involved disciplines, circuit theory, RF design, signal processing and prototyping.

The research community has widely acknowledged the MIMO systems as promising technology for future wireless networks. Therefore, different precoding schemes and techniques have been studied widely for energy and cost efficiency of the devices [31]-[33]. One of the drawbacks as compared to 4G and LTE networks, is to assign a dedicated RF chain for MIMO communication. This one RF chain includes the digital-to-analog (D/A) / analog-to-digital (A/D) converter, signal mixer and power amplifier to each antenna element in these systems, in light of the state-of-the-art hardware implementation techniques and energy consumptions.

PAAs have been used to enable new trends and paradigms for multi-antenna transmission with a single RF chain [34]. Reduction of RF chains significantly reduces energy consumption, hardware complexity, size and cost of RF circuits. It consists of one active element antenna at the center and its surrounding parasitic element antennas with adjustable reactance loads for each beam direction.

5.1 Problem formulation

PAA design

PAAs can be considered as prominent energy-efficient systems by reducing the power requirements of circuits as utilized by amplifiers, AC/DC converters and filters, etc. The array consists of a single active element and multiple parasitic elements (SAMP) tuned by load values also shown in Fig. 5.1.

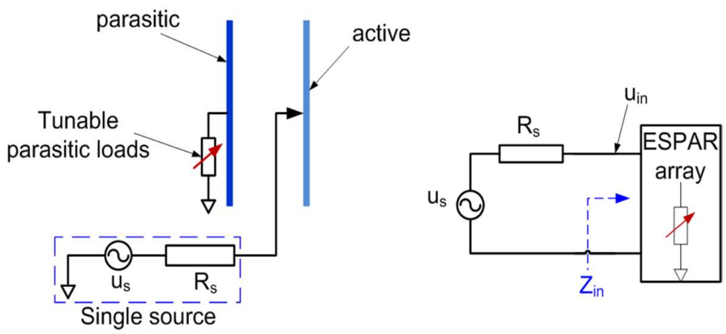

Fig. 5.1: Equivalent circuit of single active and multiple passive antenna elements.

The active element is feed through RF chain and parasitic elements receive the induced current and thus radiate. Mutual coupling is an asset here for the radiation efficiency of the array. Here coupling depends upon the distance between elements and geometry of the array structure. Desire beam direction can be achieved by tuning the load values at parasitic elements. By considering the equivalent circuit mathematical expressions can be given as;

$$\boldsymbol{i} = [\boldsymbol{Z}_m + \boldsymbol{Z}_L]^{-1}\boldsymbol{v}_s \ ,$$

$$\begin{bmatrix} Z_{11}+R_s & Z_{12} & \cdots & Z_{1m} \\ \vdots & \vdots & \ddots & \vdots \\ Z_{m1} & Z_{21} & \cdots Z_{mm} + x_{m-1} \end{bmatrix}\begin{bmatrix} I_0 \\ \vdots \\ I_m \end{bmatrix} = \begin{bmatrix} V_s \\ \vdots \\ 0 \end{bmatrix},$$

$$Z_{in} = Z_{11} + \sum_{m=2}^{N} Z_{1m}\frac{I_m}{I_0} \ ,$$

where $\boldsymbol{i}$ is the current vector $\boldsymbol{i} = [I_1, I_2, I_3, \ldots, I_M]^T$**,** containing the currents on all elements of the PAA; $\boldsymbol{Z_m} \boldsymbol{\epsilon}\ \boldsymbol{C}^{M\,X\,M}$is the mutual coupling matrix which is dependent on the PAAs geometry; $\boldsymbol{Z_L} \boldsymbol{\epsilon}\ \boldsymbol{C}^{M\,X\,M}$ is the diagonal matrix containing the complex values of the variable loads $\boldsymbol{X} = \{\boldsymbol{x_1}, \ \boldsymbol{x_2}, \ \boldsymbol{x_3}, \ldots, \ \boldsymbol{x_m}\}$ for each parasitic element and also the source resistance of each active element, which is usually 50 Ω. M is the total number of the elements of the array.

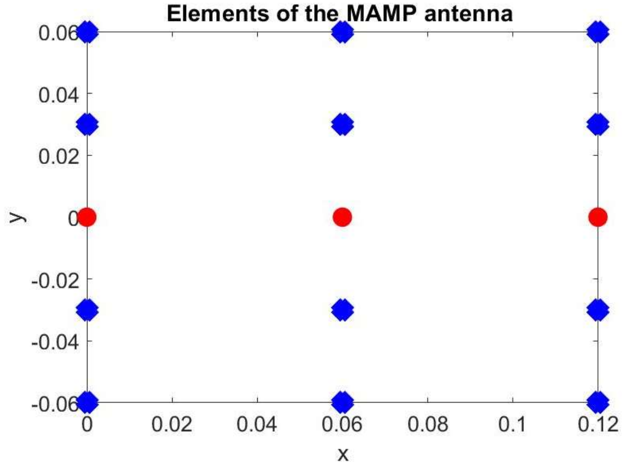

Fig. 5.2: MAMP antenna array geometry, where dots represent the active elements and the crosses represent the parasitic elements. Spacing between active elements is 0.5λ. Spacing between parasitic elements is 0.25λ

PAAs radiation constraints

As per above equations, design guidelines in the form of closed form expressions and constraints are provided in [31]. The study shows that when active elements are subject to feed and load values are set to parasitic elements for desired beam directions, then it is not the case every time that array radiates. For some load values the input impedance of the structure is less than zero, resulting in absorbing energy instead of radiating.

$$R\{Z_{in}\} < 0,$$

So, for PAAs to radiate the real value of input impedance must be greater than zero.

Multi-active/multi-passive (MAMP) antenna arrays

The performance of a PAA can be further enhanced for multi-antenna transmission by increasing the number of active elements, thus creating a MAMP antenna array. From Fig. 5.3, it can be seen that the radiation pattern from MAMPs is giving better results than a traditional uniform linear array (ULA). Where number of chains have reduced from 8 to 3.

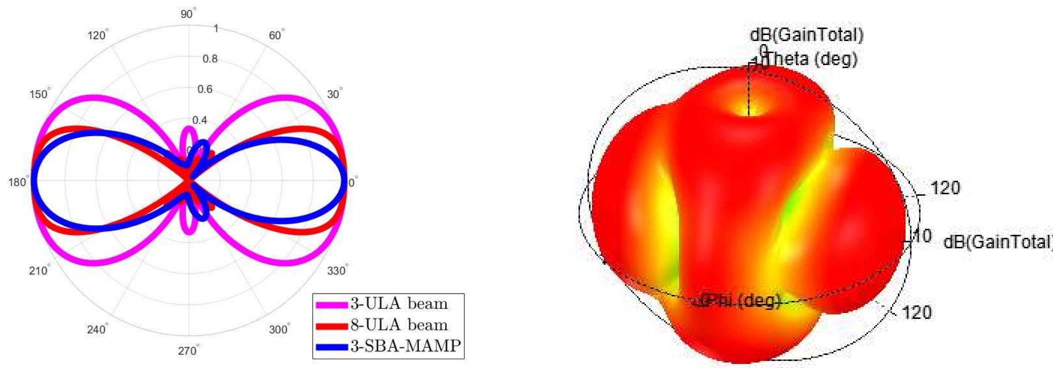

Fig. 5.3: (a) the radiation pattern of a MAMP antenna array compared with traditional Uniform Linear Array. (b) The 3D polar plot shows the radiation pattern in all planes.

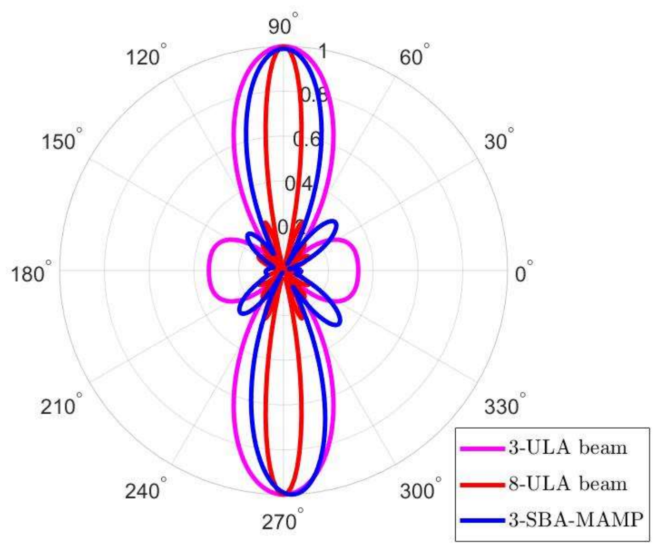

Fig. 5.4: Radiation beam directed at φ=90° by using different load values.

From the above figures i.e. Fig. 5.3 and 5.4, energy-efficient MAMPs can be a good candidate for future energy-constrained networks with directive beamforming qualities. The future work reports the investigation and the analysis performance of the proposed MAMP array in target scenario for WIPT.

6. SWIPT in mmWave cellular networks

The demand for better quality of service along with the ever increasing demand for higher data quality transmission, push the next-generation systems to provide self-sustainability to low-powered networks (e.g. sensor networks). However, for many practical communication systems, conventional EH techniques are not feasible, motivating the concept of SWIPT. Particularly, the key idea behind SWIPT is to exploit the received RF signal to obtain both information and energy. Recently, lots of works study the integration of SWIPT in numerous complex network configurations e.g., multiple-antenna systems [35], multiple-access networks [36], multiple-antenna cellular networks [37], etc. However, in realistic scenario, the interference observed between the different antennas of a receiver is spatially-correlated due to the common locations of interfering transmitters [37]. Even though the concept of SWIPT is well-investigated for multi-antenna receivers, the effect of the spatial interference correlation on the network performance was neglected. On the other hand, mmWave communication is considered as an indispensable part of the fifth- and next-generation of wireless communications owing to its abundant spectrum resources, which would lead to multi-Gbps rates. The unique features of mmWave communications, such as susceptibility to blockage, high directionality, and higher path losses, case a positive effect on the network performance, which is the mitigation of the overall interference. However, the reduced overall interference leads to a significantly lower ability to harvest sufficient RF energy [38].

In this section, we investigate a low complexity technique threshold-based Pair Switching (TbPS) for SWIPT in mmWave communications. We study the ability of SWIPT-enabled UEs to successfully decode the received signal and harvest sufficient energy in the context of mmWave communications, where UEs are equipped with multiple antennas. By using stochastic geometry tools, we study the average ID success probability and EH success probability of UEs. The joint ID and EH success probability is also investigated to show the trade-off between ID and EH of the SWIPT-enabled network. Based on the proposed TbPS scheme, we derive the optimal average radius of cells in different environments, such as urban and suburb, to give the basic guidelines for the deployment of the 5G ground BSs or UAVs.

6.1 Problem Formulation

We consider a bi-dimensional downlink mmWave cellular network. The locations of BSs are modelled based on a homogeneous Poisson Point Process (HPPP) $\Phi = \{x_i \in R^2\}$ with density of λ, where x_i denotes the spatial coordinates of the i-th node. Let r_i denote the distance between the origin and a BS at $x_i \in \Phi$. We assume that all BSs are equipped with single antenna, while all UEs have N receive antennas. The antenna array for both the transmitter and the receiver can be parametrized by three values: 1) the main lobe beam-width $\omega_m \in [0, 2\pi]$, 2) the main lobe gain G_M (dB), and 3) the side lobe gain G_S (dB). We assume that perfect beam alignment can be achieved between each UE and its serving BS by using the estimated angles of arrival, resulting in an antenna array gain of G_M. For mmWave cellular networks, a wireless link can be either in LOS or non-line-of-sight (NLOS) state, depending on whether the transmitter is visible to the receiver or not. We assume that the probability of a link to be in LOS state depends on the link's distance r_i, which is given by

$$p_{\mathrm{LOS}}(r_i) = \mathrm{H}(D - r_i)q_1 + \overline{\mathrm{H}}(D - r_i)q_2,$$

where, q_1 and q_2 are the fractions of the LOS areas inside and outside of a circle with radius D centred at the receiver, respectively. Thus, the probability of a link in NLOS state is $p_{\mathrm{NLOS}}(r_i) = 1 - p_{\mathrm{LOS}}(r_i)$. Based on the thinning property of the PPPs, the LOS and NLOS BSs form the non-homogeneous PPPs Φ_{LOS} and Φ_{NLOS} with densities $\lambda_{\mathrm{LOS}}(r_i) = p_{\mathrm{LOS}}(r_i)\lambda$ and $\lambda_{\mathrm{NLOS}}(r_i) = p_{\mathrm{NLOS}}(r_i)\lambda$, respectively. We assume that each UE communicates with its closest BS. The complementary cumulative distribution function (ccdf) of the distance R to closest BS is given by $\mathrm{P}[R \geq r] = \exp[-\pi\lambda_s(r)r^2]$, and the probability density function (pdf) of the distance R, is given by

$f_s(r) = 2\pi\lambda_s(r) r \exp(-\pi\lambda_s(r) r^2)$, where $s \in \{\mathrm{LOS}, \mathrm{NLOS}\}$. Regarding the small-scale fading, we assume Rayleigh fading with unit average power. Therefore, the power gain of the channel between the k-th antenna element of a UE and a BS is an exponential random variable with unit mean i.e., $h_{k,i} \sim \exp(1)$. For the large-scale path loss between a receiver at X ad a transmitter at Y, we assume an unbounded singular path loss model i.e., $L_s(X,Y) = \kappa_s \| X - Y \|^{\beta_s}$, where $s \in \{\mathrm{LOS}, \mathrm{NLOS}\}$, β_s is the power path loss exponent, κ_s is the path loss constant.

Even though we assume that the channels between the BSs and each antenna element of a UE are independent with each other, the received interference across different antenna elements is correlated due to the common locations of the interfering BSs. We assume that the set of antenna elements is divided into η pairs of two antenna elements i.e., $\eta = N/2$. Furthermore, we assume that the observed interference between each antenna element of a pair is fully correlated, while the intended received signals and interference between pairs are considered uncorrelated. Let S_k denote the power of the intended signal at the k-th antenna element of a UE, and I_n denote received interference power at n-th pair, where $k = \{1, \cdots, N\}$ and $n = \{1, \cdots, \eta\}$. Then, based on MRC technique, the SIR of the n-th antenna pair is given by

$$\mathrm{SIR}_n = \frac{\sum_s \left(\frac{G_M}{L_s(r_0)} h_{k,0} + \frac{G_M}{L_s(r_0)} h_{k+1,0} \right) \delta(r_0 - r_{0,s})}{\sum_s \sum_{x_i \in \Phi \backslash 0} \frac{G_M}{L_s(r_i)} h_{k,i} \mathrm{H}(r_i - r_{0,s}) \delta(r_i - r_{0,s})},$$

where, $k = 2n - 1$, $\delta(\cdot)$ is the Kronecker's delta function, $L_s(r_i)$ is the path loss function and $s \in \{\mathrm{LOS}, \mathrm{NLOS}\}$.

Regarding the selection of the number antenna pairs, ν, we adopt a threshold-based approach based on the MRC and inspired by the technique proposed in [39]. Let Γ_ν denote the post-combiner SIR for the MRC at the receiver when ν pairs of antenna elements are selected, which is equal to $\Gamma_{\nu}=\sum_{n=1}^{\nu}\mathrm{SIR}_{n}$. With the proposed TbPS scheme, the number of antenna element pairs used for ID, ν, is selected so that the Γ_{ν} exceeds a certain pre-defined threshold γ_{th} (dB), and the remaining $\eta-\nu$ pairs of antenna elements are used for EH, while satisfying the constraint that at least one pair is allocated for harvesting energy.

The conditional cdf of SIR_{n}, is given by

$$F^{s}(T\mid r_0)=1-\mathrm{L}_{I_n}\left(\ell\left(r_0,\frac{G_M}{T}\right)\right)+\ell\left(r_0,\frac{G_M}{T}\right)\frac{\partial\mathrm{L}_{I_n}\left(\ell\left(r_0,\frac{G_M}{T}\right)\right)}{\partial\ell\left(r_0,\frac{G_M}{T}\right)},$$

where, $\ell(x,\alpha)=\alpha^{-1}L_s(x)$, $s\in\{\mathrm{LOS},\mathrm{NLOS}\}$, $G\in\{G_M,G_S\}$,

$$\mathrm{L}_{I_n}(y)=\exp\left(\sum_{s}2\pi\int_{r_0}^{\infty}\lambda_s(x)\left(\phi(x,y)-1\right)x\mathrm{d}x\right),$$

$$\phi(x,y)=\sum_{G}p_G\left(1+\frac{yG}{\kappa_s x^{\beta_s}}\right)^{-1},$$

and $p_G\in\left\{\frac{\omega_m}{2\pi},\frac{2\pi-\omega_m}{2\pi}\right\}$.

Based on the proposed TbPS scheme, the ID success probability can be formulated as

$$\mathrm{F}_{\mathrm{ID}}(\chi,\gamma_{th})=\mathrm{P}\left[\Gamma_1>\chi\,\&\,\Gamma_1>\gamma_{th}\right]+\sum_{\upsilon=2}^{\eta-2}\mathrm{P}\left[\Gamma_{\upsilon}>\chi\,\&\,\Gamma_{\upsilon-1}<\gamma_{th}<\Gamma_{\upsilon}\right]+\mathrm{P}\left[\Gamma_{\eta-1}>\chi\,\&\,\Gamma_{\eta-2}<\gamma_{th}\right],$$

where χ (dB) is the decoding threshold.

The EH success probability describes the ability of a user to successfully harvest RF energy above a predefined reliability threshold Q based on the practical application. We consider a linear harvesting model, where the harvested energy is defined as the aggregated received signal power multiplied with the conversion efficiency ζ of the energy harvester. Moreover, in order to derive compact and insightful expressions for the EH success probability, we assume that the aggregate interference is dominated by the power of the strongest interfering BS. Therefore, the aggregate interference can be approximated as,

$$I_n \approx I_n^d = \sum_s \frac{h_{k,d} G}{L_s(r_d)} \delta(r_d - r_{d,s}).$$

Then, based on the number of selected pairs, ν, the EH success probability achieved by the TbPS scheme, can be formulated as,

$$\begin{aligned} \mathrm{F}_{EH}(Q,\gamma_{th}) = & \mathrm{P}\left[\Gamma_1 > \gamma_{th}\right] \mathrm{P}\left[\zeta\left(\sum_{j=1}^{\eta} S_{2j-1} + S_{2j} + 2I_j^d\right) \geq Q\right] \\ & + \sum_{\upsilon=2}^{\eta-2} \mathrm{P}\left[\Gamma_{\upsilon-1} < \gamma_{th} < \Gamma_{\upsilon}\right] \mathrm{P}\left[\zeta\left(\sum_{j=\nu+1}^{\eta} S_{2j-1} + S_{2j} + 2I_j^d\right) \geq Q\right] \\ & + \mathrm{P}\left[\Gamma_{\eta-2} < \gamma_{th}\right] \mathrm{P}\left[\zeta\left(S_{2\eta-1} + S_{2\eta} + 2I_\eta^d\right) \geq Q\right]. \end{aligned}$$

Then, we discuss the trade-off between the ID and EH in the context of the TbPS scheme, by studying the joint ID and EH success probability, $\mathrm{F}_{\mathrm{ID\&EH}}(\chi,\mathrm{Q},\gamma_{\mathrm{th}})$, which refers to the ability of a receiver to simultaneously satisfy both the ID and EH threshold. Then $\mathrm{F}_{\mathrm{ID\&EH}}(\chi,\mathrm{Q},\gamma_{\mathrm{th}})$ can be evaluated as

$$\begin{aligned} \mathrm{F}_{\mathrm{ID\&EH}}(\chi,\mathrm{Q},\gamma_{\mathrm{th}}) = & \mathrm{P}\left[\Gamma_1 > \gamma_{th} \,\&\, \Gamma_1 > \chi\right] \mathrm{P}\left[\zeta\left(\sum_{j=1}^{\eta} S_{2j-1} + S_{2j} + 2I_j^d\right) \geq Q\right] \\ & + \sum_{\upsilon=2}^{\eta-2} \mathrm{P}\left[\Gamma_{\nu} > \chi \,\&\, \Gamma_{\upsilon-1} < \gamma_{th} < \Gamma_{\upsilon}\right] \mathrm{P}\left[\zeta\left(\sum_{j=\nu+1}^{\eta} S_{2j-1} + S_{2j} + 2I_j^d\right) \geq Q\right], \\ & + \mathrm{P}\left[\Gamma_{\eta-1} > \gamma_{th} \,\&\, \Gamma_{\eta-2} < \gamma_{th}\right] \mathrm{P}\left[\zeta\left(S_{2\eta-1} + S_{2\eta} + 2I_\eta^d\right) \geq Q\right] \end{aligned}$$

For the special case with six antennas, the expressions of $\mathrm{F}_{\mathrm{ID}}(\chi,\gamma_{\mathrm{th}})$ $\mathrm{F}_{\mathrm{EH}}(\mathrm{Q},\gamma_{\mathrm{th}})$ and $\mathrm{F}_{\mathrm{ID\&EH}}(\chi,\mathrm{Q},\gamma_{\mathrm{th}})$ are given by followings:

$$\mathrm{F}_{\mathrm{ID}}(\chi,\gamma_{\mathrm{th}}) = \sum_s \int_0^\infty \mathrm{T}_{\mathrm{ID}}^{s}(r) \exp\left(-\pi\lambda_{\bar{s}}(r) r^2\right) f_s(r) \mathrm{d}r,$$

where,

$$
\begin{aligned}
&\mathrm{T}_{\mathrm{ID}}^{s}(r)\\
&=1-\overline{\mathrm{H}}(\chi-\gamma_{th})\int_0^{\chi}F^{s}(\chi-y\,|\,r)f^{s}(y\,|\,r)\mathrm{d}y\\
&-\mathrm{H}(\chi-\gamma_{th})\left(F^{s}(\chi\,|\,r)-F^{s}(\gamma_{th}\,|\,r)+F^{s}(\chi-\gamma_{th}\,|\,r)F^{s}(\gamma_{th}\,|\,r)+\int_{\chi-\gamma_{th}}^{\chi}F^{s}(\chi-y\,|\,r)f^{s}(y\,|\,r)\mathrm{d}y\right),
\end{aligned}
$$

and $s\in\{\mathrm{LOS},\mathrm{NLOS}\}$; $f^{s}(T\,|\,r_0)$ is the conditional pdf of the SIR_n, which can be calculated as $f^{s}(T\,|\,r_0)=\partial F^{s}(T\,|\,r_0)/\partial T$.

$$
\mathrm{F}_{\mathrm{EH}}(Q,\gamma_{\mathrm{th}})=\sum\nolimits_s\int_0^{\infty}\mathrm{T}_{\mathrm{EH}}^{s}(r)\exp\left(-\pi\lambda_{\bar{s}}(r)r^2\right)f_s(r)\mathrm{d}r,
$$

where,

$$
\begin{aligned}
\mathrm{T}_{\mathrm{EH}}^{s}(r)&=\left(1-F^{s}(\gamma_{th}\,|\,r)\right)H_2^{s}(Q\,|\,r)+F^{s}(\gamma_{th}\,|\,r)H_1^{s}(Q\,|\,r),\\
H_1^{s}(Q\,|\,r)&=\mathrm{L}_1\left(\ell(r_0,G_M)\right)+\ell(r_0,G_M)\frac{\partial\mathrm{L}_1\left(\ell(r_0,G_M)\right)}{\partial\ell(r_0,G_M)}\\
&\quad+\sum\nolimits_s\sum\nolimits_G\int_{r_0}^{\infty}p_G\exp\left(\overline{Q}\ell(x,2G)-\pi\lambda_{\bar{s}}(x)x^2\right)f_s^{d}(x)\mathrm{d}x,\\
H_2^{s}(Q\,|\,r)&=\sum\nolimits_{y=0}^{3}(-1)^{y}\frac{\ell^{y}(r_0,G_M)}{y!}\frac{\partial^{y}\mathrm{L}_2\left(\ell(r_0,G_M)\right)}{\partial\ell^{y}(r_0,G_M)}\\
&\quad+\sum\nolimits_s\sum\nolimits_G\int_{r_0}^{\infty}p_G\frac{1+\overline{Q}\ell(x,2G)}{\exp\left(\overline{Q}\ell(x,2G)+\pi\lambda_{\bar{s}}(x)x^2\right)}f_s^{d}(x)\mathrm{d}x,
\end{aligned}
$$

$$
\mathrm{L}_1(y)=\exp(-\overline{Q}y)\sum\nolimits_s\sum\nolimits_G\int_{r_0}^{\infty}p_G\gamma^{-1}(x,y)\left(1-\exp(-\overline{Q}\ell(x,2G)\gamma(x,y))\right)\exp(-\pi\lambda_{\bar{s}}(x)x^2)f_s^{d}(x)\mathrm{d}x,
$$

$$
\mathrm{L}_2(y)=\exp(-\overline{Q}y)\sum\nolimits_s\sum\nolimits_G\int_{r_0}^{\infty}p_G\gamma^{-2}(x,y)\frac{1+\exp\left(-\overline{Q}\ell(x,2G)\gamma(x,y)\right)\left(1+\overline{Q}\ell(x,2G)\gamma(x,y)\right)}{\exp(-\pi\lambda_{\bar{s}}(x)x^2)}f_s^{d}(x)\mathrm{d}x,
$$

where, $s\in\{\mathrm{LOS},\mathrm{NLOS}\}$, $G\in\{G_M,G_S\}$ and $p_G\in\{\frac{\omega_m}{2\pi},\frac{2\pi-\omega_m}{2\pi}\}$; $\ell(x,\alpha)=\alpha^{-1}L_s(x)$ and $\gamma(x,y)=1-y/\ell(x,2G)$.

$$
\mathrm{F}_{\mathrm{ID}}(\chi,Q,\gamma_{\mathrm{th}})=\sum\nolimits_s\int_0^{\infty}\mathrm{T}_{\mathrm{ID\&EH}}^{s}(r)\exp\left(-\pi\lambda_{\bar{s}}(r)r^2\right)f_s(r)\mathrm{d}r,
$$

where,

$$\begin{aligned}&\mathrm{T}^{s}_{\mathrm{ID\&EH}}(r)\\&=\mathrm{H}(\chi-\gamma_{th})\left(H_2^s(Q\,|\,r)\overline{F}^{s}(\gamma_{th}\,|\,r)\overline{F}^{s}(\chi\,|\,r)+H_1^s(Q\,|\,r)F^s(\gamma_{th}\,|\,r)\int_0^{\gamma_{th}}F^s(\chi-y\,|\,r)f^s(y\,|\,r)\mathrm{d}y\right)\\&+\overline{\mathrm{H}}(\chi-\gamma_{th})\left(H_2^s(Q\,|\,r)\overline{F}^{s}(\gamma_{th}\,|\,r)+H_1^s(Q\,|\,r)F^s(\gamma_{th}\,|\,r)(1-H_1^s(Q\,|\,r))\int_0^{\chi}F^s(\chi-y\,|\,r)f^s(y\,|\,r)\mathrm{d}y\right),\end{aligned}$$

$s\in\{\mathrm{LOS},\mathrm{NLOS}\}$ and $\overline{F}^s(\cdot)=1-F^s(\cdot)$.

6.2 Numerical Results

In this section, we provide the numerical results to validate the accuracy of our model and illustrate the performance of the TbPS scheme. The system parameters are given by following table,

Table. 6.1: System parameters

λ	$1/(2500\pi)$ BS/m^2
q_1	0.9
q_2	0.75
D	100 m
β_{LOS}	3
β_{NLOS}	4
G_M	6
G_S	0.24
ζ	0.7

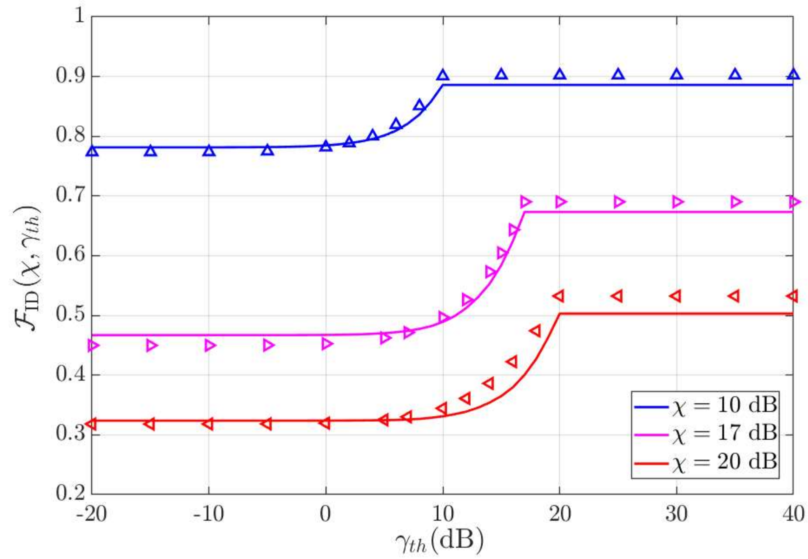

Fig. 6.1: ID success probability versus the threshold γ_{th} for different $\chi \in \{10, 17, 20\}$ dB

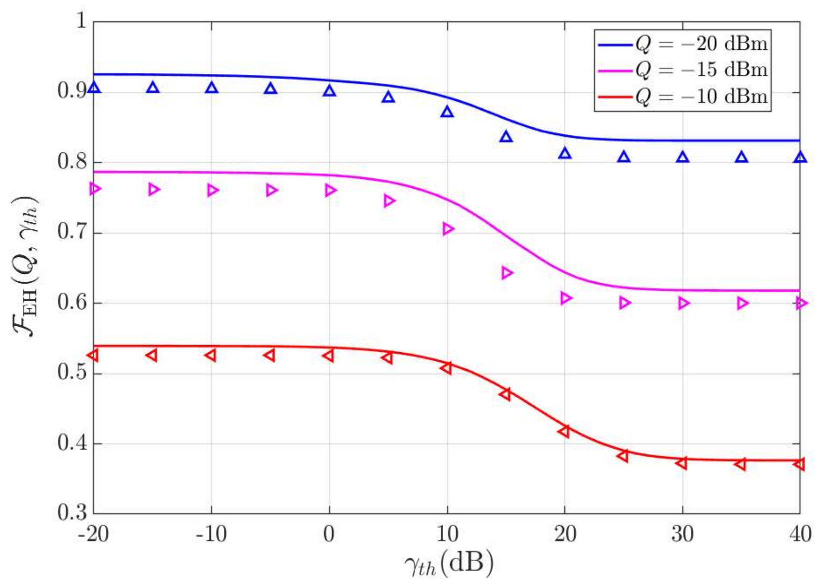

Fig. 6.2: EH success probability versus the threshold γ_{th} for different $Q \in \{-10, -15, -20\}$ dBm

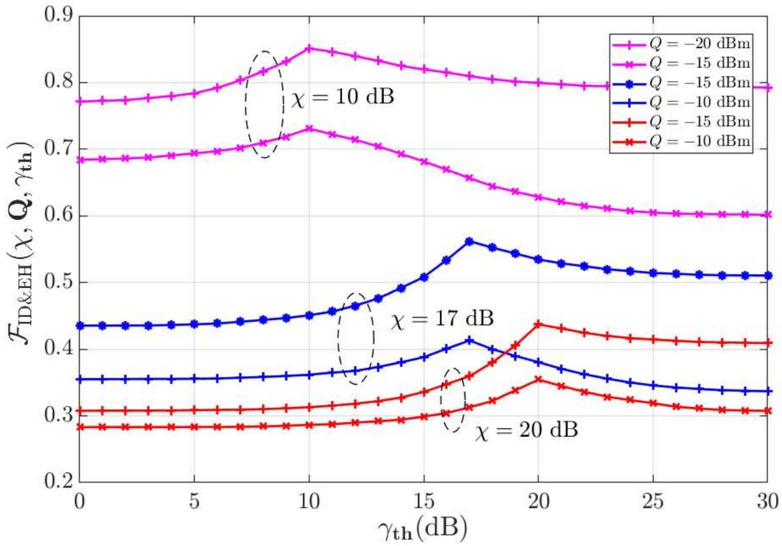

Fig. 6.3: Joint ID and EH success probability versus the threshold γ_{th} for different dB χ and Q.

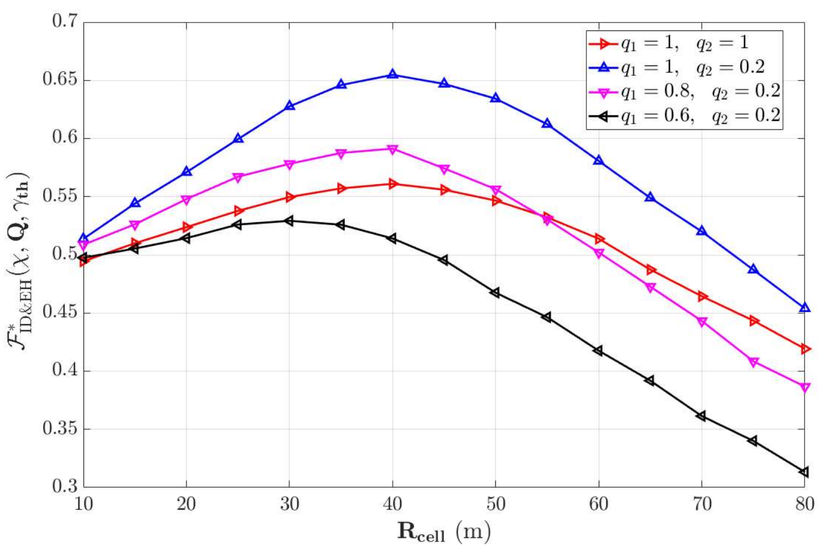

Fig. 6.4: Joint ID and EH success probability versus the BSs density λ for different blockages characteristics.

Fig 6.1 illustrates the effect of the threshold γ_{th} on the ability of a UE to successfully decode the received signal power. In particular, Fig 6.1 plots the ID success probability with respect to the threshold γ_{th} for different decoding thresholds $\chi \in \{10, 17, 20\}$ dB. We can easily observe that, the ability of a UE to successfully decode the received signal power increases with the increase of the predefined threshold γ_{th} This was expected since, the increase of γ_{th} results in an increased number of antenna elements that perform ID, and consequently, the ability to successfully decode the received signal power is enhanced. However, beyond a critical value of γ_{th}, which is equal to $\gamma_{th} = \chi$, the ID success probability remains constant. This is can be explained by the fact that, for large values of γ_{th}, a UE is unable to assign an additional pair of antennas for the ID due to the constrain of the existence of at least one pair of antennas for EH. Similarly, Fig 6.2 illustrates the effect of γ_{th} on the EH success probability for different reliability thresholds $Q \in \{-10, -15, -20\}$ dBm. As expected, the harvested energy of UE decreases as the predefined threshold γ_{th} increases, since the number of antenna elements allocated for EH reduces, and hence the EH success probability drops. Moreover, Fig. 6.2 demonstrates the impact of the considered approximation regarding the observed interference on the EH success probability. The small deviation from the theoretical curves shows that the overall network interference can be effectively approximated by the interference caused by the strongest BS, without being significantly deficient in accuracy. Finally, the agreement between the theoretical curves (solid lines) and the simulation results (markers) in both figures. validates our mathematical analysis.

Fig. 6.3 shows the impact of the threshold γ_{th} on the ability of a UE to simultaneously satisfy the requirements for both ID and EH procedures. It is interesting to note that, by increasing the threshold γ_{th}, the ability of a user to simultaneously satisfy the ID and EH constrains increases. This is because, as the value of the threshold γ_{th} increases, the proposed TbPS scheme allocates a higher number of antenna elements for the ID part. Hence, the ability of a user to successfully decode the received signal is significantly improved, while its ability to harvest energy is slightly reduced. However, beyond the critical point $\gamma_{th} = \chi$, the ability of a user to simultaneously satisfy the ID and EH constrains decreases.

As indicated in Fig. 6.1 and Fig. 6.2, the ability of a user to successfully decode the received signal beyond a threshold equal to $\gamma_{th} = \chi$, remains constant, while the ability to harvest energy is reducing, and hence the joint ID and EH success probability is decreasing.

Fig. 6.4. illustrates the effect of the density on the optimal joint ID and EH success probability for rural (no blockage effects i.e., $q_1 = 1$ and $q_2 = 1$) and urban (with blockage effects i.e., $0 \le q_2 < q_1 \le 1$) scenarios, where $\chi = \gamma_{th} = 17$dB and $Q = -15$ dBm; the radius of the cell $R_{cell} = (\pi\lambda)^{-1/2}$ m. As expected, the existence of blockages negatively affects the performance and as a result reduces the ability of UE to jointly satisfy the ID and EH constrains. Although the existence of blockages reduces the aggregate network interference, the overall harvested energy by UE is significantly reduced, and hence the joint ID and EH success probability decreases. Another interesting observation is that, for low density values, the joint ID and EH success probability increases with the increasing number of BSs. This again is expected, since by increasing the BS density, more and more BSs are deployed within the network, resulting in an improved SIR at the UE as well as an enhanced harvested energy. However, by further increasing the BS density, a significant loss in the joint ID and EH success probability can be observed, due to the significant increase of the network interference. This critical density value, that maximizes the ability of a UE to jointly satisfy the ID and EH constrains, decreases as the blockage effects within the network increase i.e., small-cell deployment is beneficial for environments with high density of blockages.

7 Future Plans

As it can be easily observed, the proposed target scenario for the first phase integrates different components, such as rectenna design for WIPT, a cooperative multi-hop relaying network using UAVs, advanced diversity schemes with a simple EH model and deployment of the most recent state-of-art IRSs. Each part will be investigated in more detail to discover its impact on the overall network performance.

More specifically, the model shown in Fig. 3.1 will be adapted to the current analysis, with the inclusion of the EH part to the proposed cooperative multi-hop relaying network. For the implementation of WPT, the system could use either the WPCN or the SWIPT operation for powering the relays. Moreover, a multiple-level rechargeable battery for each relay could be considered. This could be combined with an adaptive myopic coding protocol for the transmission of the signals through the network. For these topics, the performance of the system will be investigated in terms of outage probability, diversity gain, and energy efficiency, and some optimization problems will be considered, such as the minimization of the transmit power for the EH part concerning the PS or the TS parameters.

Furthermore, we aim to develop our system model to optimize both Sum Rate and Total Harvested Energy, considering a minimum requirement of service quality to be provided to the user, such as the minimum data rate and minimum harvested energy. Besides, we know that RISs have a preferable impact on the propagation channel, improving communication link quality. In order to reap up these benefits, RISs should be appropriately designed. Thereby, we have to take into account hardware impairment of RISs and circuit design for EH such as the effect of different receiver configurations based on power splitting, time switching, antenna switching, and non-linear EH model.

For the antenna design, the future work reports the investigation and the analysis performance of the proposed MAMP array in rectenna for WIPT. The plan is to design a highly directive and high gain antenna array that will be the right candidate for the transmission as well as for EH. To cope with state-of-the-art communication systems, i.e., 5G, the array must be designed for the mmWave frequencies to support the high data rates. This study might include designing of IRS to fulfil the needs of this proposed research. We aim to optimize the phases at Relay BS and IRS by minimizing the total utilized power in the system through antenna array. The study also targets the formulation and solution of new problems on how to minimize the communication power and to enhance the performance of EH systems using proposed WIPT techniques.

Then, based on SWIPT-enabled mmWave cellular networks, we will investigate other advanced diversity schemes by using order statistics. Meanwhile, we will integrate the IRS in the network-level analysis to further enhance the system performance. For simplicity purposes, a linear EH model is used in the first phase of the "Energy Harvesting techniques and network-level optimization." In the second phase, we will investigate the non-linear EH model to obtain more practical results. Given the complicated analytical process, system optimization becomes a tough work. Hence, proper simplification of system elements, such as other-cell interference, will be further studied.

The design of a highly directive and high gain antenna array at the BS will reduce the consumed energy and deliver more energy at the targeted receiver. Moreover, the cooperative multi-hop relay consists of UAVs with a multiple-level rechargeable battery that will be an enabling factor for extending cell coverage and provide adequate QoS for cell-edge users. RIS can focus the incident electromagnetic RF signals upon its surface to create an energy or information hot spot zone. The combined use of these technologies will enhance the performance of mmWave networks, since severe path loss and NLOS conditions could be avoided. Spectral, energy efficiencies, outage probability, and other system performance indicators will be measured to indicate the whole system performance. These measurements will be studied under different system configurations and requirements. Different receiver configurations based on power splitting, time switching, antenna switching, nonlinear EH model, waveform signal design, the minimum data rate, minimum harvested energy, and hardware impairment of RISs constraints will be considered.

References

[1]. V. Chamola and B. Sikdar, "Solar powered cellular base stations: current scenario, issues and proposed solutions," in *IEEE Commun. Mag.*, vol. 54, no. 5, pp. 108-114, May 2016.

[2]. Q. Wu, G. Y. Li, W. Chen, D. W. K. Ng, and R. Schober, "An overview of sustainable green 5G networks," in *IEEE Wireless Commun.*, vol. 24, no. 4, pp. 72-80, Aug. 2017.

[3]. I. Krikidis, S. Timotheou, S. Nikolaou, G. Zheng, D. W. K. Ng, and R. Schober, "Simultaneous wireless information and power transfer in modern communication systems," in *IEEE Commun. Mag.*, vol. 52, no. 11, pp. 104-110, Nov. 2014.

[4]. X. Zhou, R. Zhang and C. K. Ho, "Wireless information and power transfer: architecture design and rate-energy tradeoff," in *IEEE Trans. Commun.*, vol. 61, no. 11, pp. 4754-4767, Nov. 2013.

[5]. R. Zhang and C. K. Ho, "MIMO broadcasting for simultaneous wireless information and power transfer," in *IEEE Trans. Wireless Commun.*, vol. 12, no. 5, pp. 1989-2001, May 2013.

[6]. B. Clerckx, R. Zhang, R. Schober, D. W. K. Ng, D. I. Kim, and H. V. Poor, "Fundamentals of wireless information and power transfer: from RF energy harvester models to signal and system designs," *IEEE J. Sel. Areas Commun*., vol. 37, no. 1, pp. 4-33, Jan. 2019.

[7]. Chelli, K. Kansanen, M. Alouini, and I. Balasingham, "On bit error probability and power optimization in multihop millimeter wave relay systems," *IEEE Access*, vol. 6, pp. 3794-3808, Jan. 2018.

[8]. S. Sudevalayam and P. Kulkarni, "Energy harvesting sensor nodes: survey and implications," *IEEE Commun. Surveys Tuts.*, vol. 13, no. 3, pp. 443-461, Sep. 2011.

[9]. S. Bi, Y. Zeng and R. Zhang, "Wireless powered communication networks: an overview," *IEEE Wireless Commun.*, vol. 23, no. 2, pp. 10-18, Apr. 2016.

[10]. M. O. Hasna and M. Alouini, "Outage probability of multihop transmission over Nakagami fading channels," *IEEE Commun. Lett*., vol. 7, no. 5, pp. 216-218, May 2003.

[11]. V. Jamali, N. Zlatanov, H. Shoukry, and R. Schober, "Achievable rate of the half-duplex multi-hop buffer-aided relay channel with block fading," *IEEE Trans. Wireless Commun.*, vol. 14, no. 11, pp. 6240-6256, Nov. 2015.

[12]. J. Boyer, D. D. Falconer and H. Yanikomeroglu, "Multihop diversity in wireless relaying channels," *IEEE Trans. Commun*., vol. 52, no. 10, pp. 1820-1830, Oct. 2004.

[13]. L. Ong and M. Motani, "Myopic coding in multiterminal networks," *IEEE Trans. Inf. Theory*, vol. 54, no. 7, pp. 3295-3314, Jul. 2008.

[14]. D. K. P. Asiedu, H. Lee and K. Lee, "Simultaneous wireless information and power transfer for decode-and-forward multihop relay systems in energy-constrained IoT networks," *IEEE Internet Things J.*, vol. 6, no. 6, pp. 9413-9426, Dec. 2019.

[15]. W. Xu, W. Cheng, Y. Zhang, Q. Shi, and X. Wang, "On the optimization model for multi-hop information transmission and energy transfer in TDMA-based wireless sensor networks," *IEEE Commun. Lett.*, vol. 21, no. 5, pp. 1095-1098, May 2017.

[16]. J. Gil-Pelaez, "Note on the inversion theorem," Biometrika, vol. 38, no. 3-4, pp. 481-482, Dec. 1951.

[17]. M. D. Renzo, M. Debbah, D. T. Phan-Huy, A. Zappone, M. S. Alouini, C. Yuen, V. Sciancalepore, G. C. Alexandropoulos, J. Hoydis, H. Gacanin, J. de Rosny, A. Bounceur, G. Lerosey, and M. Fink, "Smart radio environments empowered by reconfigurable AI metasurfaces: an idea whose time has come," *Eurasip J. Wireless Commun. and Net.*, vol. 2019, no. 1, May 2019.

[18]. Q. Wu and R. Zhang, "Towards Smart and Reconfigurable Environment: Intelligent Reflecting Surface Aided Wireless Network," in *IEEE Commun. Mag.*, vol. 58, no. 1, pp. 106-112, Jan. 2020.

[19]. Q. Wu and R. Zhang, "Intelligent reflecting surface enhanced wireless network via joint active and passive beamforming," in *IEEE Trans. Wireless Commun.*, vol. 18, no. 11, pp. 5394-5409, Nov. 2019.

[20]. X. Yu, D. Xu, and R. Schober, "MISO wireless communication systems via intelligent reflecting surfaces: (Invited paper)," in *Proc. IEEE/CIC Int. Conf. Commun. in China (ICCC)*, pp. 735–740, Aug. 2019.

[21]. H. Guo, Y. Liang, J. Chen, and E. G. Larsson, "Weighted sum-rate maximization for reconfigurable intelligent surface aided wireless networks," in *IEEE Trans. Wireless Commun.*, vol. 19, no. 5, pp. 3064-3076, May 2020.

[22]. G. Zhou, C. Pan, H. Ren, K. Wang, M. Di Renzo, and A. Nallanathan, "Robust beamforming design for intelligent reflecting surface aided MISO communication systems," in *IEEE Wireless Commun. Lett. (Early Access)*.

[23]. G. Zhou, C. Pan, H. Ren, K. Wang, and A. Nallanathan, "Intelligent reflecting surface aided multigroup multicast MISO communication systems," in *IEEE Trans. Signal Process.*, vol. 68, pp. 3236-3251, Apr. 2020.

[24]. X. Li, J. Fang, F. Gao, and H. Li, "Joint active and passive beamforming for intelligent reflecting surface-assisted massive MIMO systems," *arXiv preprint arXiv:1912.00728*, Dec. 2019.

[25]. X. Yu, D. Xu, and R. Schober, "Optimal beamforming for MISO communications via intelligent reflecting surfaces," *arXiv preprint arXiv: 2001.11429*, 2020.

[26]. L. Wei, C. Huang, G. C. Alexandropoulos, and C. Yuen, "Parallel factor decomposition channel estimation in RIS-assisted multi-user MISO communication," in *Proc. 11th IEEE Sensor Array and Multichannel Signal Processing Workshop (SAM)*, Hangzhou, China, Jun. 2020, pp. 1-5.

[27]. G. C. Alexandropoulos and E. Vlachos, "A hardware architecture for reconfigurable intelligent surfaces with minimal active elements for explicit channel estimation," in *Proc. IEEE Int. Conf. Acoustics, Speech and Signal Process. (ICASSP)*, Barcelona, Spain, May 2020, pp. 9175-9179.

[28]. Q. Wu and R. Zhang, "Weighted sum power maximization for intelligent reflecting surface aided SWIPT," in *IEEE Wireless Commun. Lett.*, vol. 9, no. 5, pp. 586-590, May 2020.

[29]. Y. Tang, G. Ma, H. Xie, J. Xu, and X. Han, "Joint transmit and reflective beamforming design for IRS-assisted multiuser MISO SWIPT systems," in *Proc. IEEE Int. Conf. Commun. (ICC)*, Dublin, Ireland, Jun. 2020, pp. 1-6.

[30]. Q. Wu and R. Zhang, "Joint active and passive beamforming optimization for intelligent reflecting surface assisted SWIPT under QoS constraints," in *IEEE J. Sel. Areas Commun. (Early Access).*

[31]. A. Li, C. Masouros and C. B. Papadias, "MIMO transmission for single-fed ESPAR with quantized loads," in *IEEE Trans. Commun.*, vol. 65, no. 7, pp. 2863-2876, Jul. 2017.

[32]. M. Costa, "Writing on dirty paper," in *IEEE Trans. Inf. Theory*, vol. 29, no. 3, pp. 439-441, May 1983.

[33]. M. C. Lee, W. H. Chung, and T. S. Lee, "Generalized precoder design formulation and iterative algorithm for spatial modulation in MIMO systems with CSIT," in *IEEE Trans. Commun*., vol. 63, no. 4, pp. 1230–1244, Apr. 2015.

[34]. A. Kalis, A. G. Kanatas, C. B. Papadias, *Parasitic antenna arrays for wireless MIMO systems*, *Springer* 2014.

[35]. T. Tu Lam, M. Di Renzo and J. P. Coon, "System-level analysis of SWIPT MIMO cellular networks," in *IEEE Commun. Lett.,* vol. 20, no. 10, pp. 2011-2014, Oct. 2016.

[36]. S. Belhadj Amor, S. M. Perlaza, I. Krikidis, and H. V. Poor, "Feedback enhances simultaneous wireless information and energy transmission in multiple access channels," in *IEEE Trans. Inf. Theory*, vol. 63, no. 8, pp. 5244-5265, Aug. 2017.

[37]. R. Tanbourgi, H. S. Dhillon, J. G. Andrews, and F. K. Jondral, "Effect of spatial interference correlation on the performance of maximum ratio combining," in *IEEE Trans. Commun.,* vol. 13, no. 6, pp. 3307-3316, Jun. 2014.

[38]. Y. Niu, Y. Li, D. Jin, L. Su, and A. Vasilakos, "A survey of millimeter wave communications (mmWave) for 5G: opportunities and challenges", *Wireless Networks*, vol. 21, no. 8, pp. 2657-2676, Apr. 2015.

[39]. F. Benkhelifa and M. Alouini, "Prioritizing data/energy thresholding-based antenna switching for SWIPT-enabled secondary receiver in cognitive radio networks," *IEEE Trans. Commun.,* vol. 3, no. 4, pp. 782–800, Dec. 2017.